Korean J. Chem. Eng., 34(5), 1416-1434 (2017)
DOI: 10.1007/s11814-017-0021-5

pISSN: 0256-1115
eISSN: 1975-7220

Separation of tetrahydrofuran using RSM optimized accelerator-sulfur-filler of rubber membranes: Systematic optimization and comprehensive mechanistic study

Mrinmoy Karmakar, Manas Mahapatra, and Nayan Ranjan Singha†

Department of Polymer Science and Technology, Advanced Polymer Laboratory,
Government College of Engineering and Leather Technology (Post-Graduate),
Maulana Abul Kalam Azad University of Technology, Salt Lake, Kolkata - 700106, West Bengal, India
(*Received 1 October 2016 • accepted 6 February 2017*)

Abstract−Response surface methodology (RSM) optimized, semi efficiently vulcanized (SEV) and filled organophilic composite natural rubber (NR) membranes of varying physichochemical interactions were reported for sorption-diffusion-permeation based separation of tetrahydrofuran (THF) from binary aqueous mixtures. RSM was used to obtain optimum accelerator/sulfur (A/S) ratio required for crosslinking of nine membranes to find excellent balance of mechanical properties. These membranes were characterized by FESEM, AFM, EDX, XRD, DTG, TGA, DSC and FTIR. Vulcanized products formed from several crosslinking precursors of NR via radical and/or ionic paths were incorporated to impart an unambiguous reaction mechanism. RSM was also used to obtain optimum conditions (temperature/concentration/filler) for total flux (TF) and separation factor (SF). Membrane intrinsic properties, like partial permeabilities (PPs), selectivities and diffusion coefficients (DCs) were also studied. NRSEV12 membrane showed excellent balance of TF (24.01 ± 0.7 g m^{-2} h^{-1}) and SF (118.8 ± 4.16) at 0.97 wt% of THF in feed and 35 °C.

Keywords: Accelerator/Sulfur Ratio of Vulcanization, Advanced Characterization, Systematic Optimization of Property-performance, Intrinsic Properties of Composite Membranes, Reaction Mechanism

INTRODUCTION

Pervaporation (PV) is a widely used membrane based technique for dehydration [1], separation of azeotropic mixtures [2], close-boiling mixtures [3] and recovery of traces of impurities from aqueous solutions [4]. Membrane based separation has gained much attention for its high selectivity, low energy consumption, moderate cost to performance ratio and compact modular design. The chemical potential gradient across the membrane is the driving force for the mass transport in PV.

Tetrahydrofuran (THF) is a colourless heterocyclic ether possessing low viscosity, potential basicity, moderate water solubility, high dielectric constant (7.6) and dipole moment of 1.63 D, which enables it to dissolve a wide range of polar components. It forms azeotrope at 63.9 °C and 94.3 wt% of in water [5]. Its density and solubility parameter (SP) are 0.8892 g cm^{-3} and 19.2 $MPa^{0.5}$, respectively. THF is extensively used as an expensive solvent to dissolve different monomers and polymers, as well as in different chemical reactions, including hydroboration and Grignard reactions [6]. Besides, THF finds its applications in liquid chromatography as mobile phase and as an intermediate or a monomer in manufacturing colours, glues, colour toners and therapeutic products [2,7]. Therefore, waste effluents of these industries contain dissolved THF and hence recycling has become an essential task to reduce the industrial investment. However, conventional distillation does not give high separation due to the formation of azeotrope. Again, the tendency of THF to produce unstable peroxides in contact with aerial oxygen may cause explosion during distillation [2].

Use of hydrophilic membranes, made of various homo- and co-polymers [8,9], polymeric blends [10-12] and polymer-inorganic composites [13-16], have already been studied for dehydrating THF. However, the recovery of THF from aqueous solution is limited [2,17-19], owing to the lack of available THF selective organophilic membranes.

In case of elastomers, the amorphous nature limits their use as organophilic membranes due to high flux but poor organic selectivity. Vulcanization can solve this problem via enhancing elasticity of raw rubber (NR) and offering good balance between tensile strength (TS) and elongation at break (EAB). The hardness and abrasion resistance also get increased during vulcanization, which thereby makes vulcanized NR more applicable than uncured NR for removing of organics from their binary aqueous solutions, depending upon the closeness of solubility parameters between membranes and organics.

Though few works have been devoted to the use of RSM towards membrane based PV process [20-23], its use towards optimizing the of pervaporative removal of THF from THF-water system using carbon black filler (CBF) filled and sulfur crosslinked NR membranes has not yet been reported. In fact, membrane properties are found to vary significantly even after the small changes in either A/S or the wt% of filler. Thus, the prevalence of optimum physicochemical properties can only be possible by the incorporation of optimum amounts of filler, accelerator and sulfur, obtained by RSM. In this context, though some attempts have been made to get the optimum balance of these aforesaid properties by gradual addition

†To whom correspondence should be addressed.
E-mail: drs.nrs@gmail.com

of these ingredients in different amounts to synthesize membranes of varying CDs and crystallinity, followed by the measurements of physicochemical properties or characterization by several conventional methods to avoid the appearance of either very high CDs or formation of filler aggregates, the exact balance of physicochemical properties of membranes, as required in pervaporative separation, using two steps optimization method has not yet been reported.

Like other chemical reactions, rubber vulcanization also depends on several physical parameters, such as temperature, solubility, relative strengths, pH and chemical nature of the vulcanizing agent [24]. Accelerated sulfur vulcanization has been found to impart excellent strength, dynamics and lowest curing cost. Although several works have been carried out to understand the type and mechanism of vulcanization between rubber and vulcanizing agents [25, 26], an unambiguous mechanism of such reaction is yet to be established. In the present study, NR was vulcanized by sulfur through SEV method using zinc diethyldithiocarbamate (ZDC) as the accelerator and filled by varying doses of CBF to produce four new (i.e., NRSEV0, NRSEV8, NRSEV12 and NRSEV24) crosslinked/composite membranes. We found both radical and ionic paths for accelerated sulfur vulcanization of NR for the formation of different crosslink precursors and different vulcanized products from these precursors. In the present work, all possible mechanisms of accelerated sulfur vulcanization of NR have been incorporated to explain the vulcanization reaction properly. Previously, efficiently vulcanized SBR (SBREV) and NR (NREV) membranes were tried for the recovery of traces of pyridine from pyridine/water systems [3,27]. However, RSM optimization has established NRSEV to have the best balance of the mechanical properties. Thus, in the present work, unfilled and filled NRSEV membranes have been used for the pervaporative removal of THF from THF-water mixtures along with the optimization of their potential performance in PV by RSM, ensuring interactive effects of temperature, wt% of THF and wt% of filler.

EXPERIMENTAL

1. Theory

1-1. Thermodynamics of Sorption

Interaction parameters (IPs) between solvents in feed (χ_{ij}^{f}) and membrane (χ_{ij}^{m}), help determine the relative sorption of THF and water by the elastomeric membranes, of which χ_{ij}^{f} can be determined using Eq. (1a) based on Flory-Huggins thermodynamics [24].

$$\chi_{ij}^{f}=\frac{1}{x_i v_j}\left[x_i \ln\left(\frac{x_i}{v_i}\right)+x_j \ln\left(\frac{x_j}{v_j}\right)+(x_i \ln\gamma_i+x_j \ln\gamma_j)\right] \tag{1a}$$

Here, v_i/x_i and v_j/x_j are volume fractions/mole fractions (VFs/MFs) of THF (i) and water (j) in feed mixture, respectively. For determining IP between solvents in membrane (χ_{ij}^{m}), χ_{ij}^{f} is first plotted against feed VF (v_i) of i to obtain a polynomial trend line. IPs of i and j in membrane and feed are obtained from VFs of components using a method reported elsewhere [28]. IP between solvent (i) and membrane (χ_{ip}) is obtained from VF of polymer (ϕ_p) using Eq. (1b).

$$\chi_{ip}=\frac{-\ln(1-\varphi_p)-\varphi_p}{\varphi_p^2} \tag{1b}$$

The activity coefficients of i and j for different feed mixtures are determined by two parameters Wilson equations (Eqs. (2a) and (2b)) [29].

$$\ln\gamma_i=-\ln(x_i+\Lambda_{ij}x_j)+x_j\left(\frac{\Lambda_{ij}}{x_i+\Lambda_{ij}x_j}-\frac{\Lambda_{ji}}{x_j+\Lambda_{ji}x_i}\right) \tag{2a}$$

$$\ln\gamma_j=-\ln(x_j+\Lambda_{ji}x_i)-x_i\left(\frac{\Lambda_{ij}}{x_i+\Lambda_{ij}x_j}-\frac{\Lambda_{ji}}{x_j+\Lambda_{ji}x_i}\right) \tag{2b}$$

The Wilson parameters (Λ_{ij} and Λ_{ji} for i and j) are obtained from its vapor-liquid-equilibrium (VLE) data [30]. Though solubility parameters of various solvents and polymers are available in literature, it can still be varied for attainment of chemical (crosslinking) and physical (filler loading) modifications. Solubility parameters of membranes (δ_p) are obtained from IPs by Eq. (3) [24].

$$\chi_{ip}=0.35+\frac{V_i}{RT}(\delta_i-\delta_p)^2 \tag{3}$$

Here, V_i is molar volume and δ_i is solubility parameter of i. Membrane phase activity of i (a_i) for binary sorption (membrane and one solvent) is obtained using Eq. (4) based on Flory-Huggins thermodynamics.

$$\ln a_i=\ln(1-\varphi_p)+\varphi_p+\chi_{ip}\varphi_p^2 \tag{4}$$

However, mole fraction of i within membrane is difficult to measure, since polymer possesses molecular weight distribution instead of fixed molecular weight. Assuming constant density of components and polymer within membrane, MF may be replaced by VF. Accordingly, activity of i within membrane may be assumed by Eq. (5a).

$$a_i^m=\varphi_i^m\gamma_i^m \tag{5a}$$

Here, φ_i^m is VF of i within membrane. For a single component sorption by membrane, $a_i^m=1$ and activity coefficient for single component in membrane (state-I) can be calculated using Eq. (5b).

$$\gamma_i^m=\frac{1}{\varphi_i^m} \tag{5b}$$

In fact, state-II helps determine the coupling of each component with membrane without the aid of interactive effect between i and j. The state-II activity coefficient of i in binary mixtures of i and j can be calculated using Eq. (5c).

$$\ln\gamma_i^m=\varphi_p+\chi_{ip}\varphi_p^2=(1-\varphi_i)+\chi_{ip}(1-\varphi_i)^2 \tag{5c}$$

Again, considering coupling effect, activity coefficients of i and j (i.e. state-III) may be obtained by Eqs. (5d) and (5e).

$$\ln\gamma_i^m=\varphi_p+\chi_{ip}\varphi_p^2+\left(1-\frac{V_i}{V_j}\right)\varphi_j+\chi_{ij}\varphi_j^2+\left(\chi_{ij}+\chi_{ip}-\frac{V_i}{V_j}\chi_{jp}\right)\varphi_j\varphi_p-u_i u_j\varphi_j\frac{\delta\chi_{ij}}{\delta u_j} \tag{5d}$$

$$\ln\gamma_j^m=\varphi_p+\chi_{jp}\varphi_p^2+\left(1-\frac{V_j}{V_i}\right)\varphi_i+\frac{V_j}{V_i}\chi_{ij}\varphi_i^2+\frac{V_j}{V_i}\left(\chi_{ij}-\chi_{ip}+\frac{V_i}{V_j}\chi_{jp}\right)\varphi_i\varphi_p+\frac{V_j}{V_i}u_i^2\varphi_j\frac{\delta\chi_{ij}}{\delta u_j} \tag{5e}$$

Here, u_i/u_j represent VFs of i/j that can be obtained by Eqs. (5f)

and (5g).

$$u_i = \frac{\varphi_i}{\varphi_i + \varphi_j} \tag{5f}$$

$$u_j = \frac{\varphi_j}{\varphi_i + \varphi_j} \tag{5g}$$

1-2. Measurement of Partial Permeabilities (PPs) and Membrane Selectivities (MSs)

Based on solution-diffusion model, mass flux of i through a dense PV membrane may be described in terms of its vapor pressure (VP) difference (driving force) on feed and permeate sides by Eq. (6).

$$J_i = \frac{P_i}{l}(p_f - p_p) \tag{6}$$

Here, l is membrane thickness; p_f and p_p are VPs of feed and permeate sides, respectively. P_i is intrinsic membrane permeability and P_i/l is membrane permeance [24]. VP of i on feed side (p_f) i.e. fugacity of it (f_i) may be obtained using Eq. (7).

$$p_f = x_i \gamma_i p_s = f_i \tag{7}$$

Here, $p_s/x_i/y_i$ are saturated vapor pressure/mole fraction/activity coefficient of i on feed side. Due to extreme low pressure, the components at permeate side may be assumed to behave like an ideal gas. Thus, partial VP of i on permeate side (p_p) may be obtained using Eq. (8) [31].

$$P_p = y_i P_p \tag{8}$$

Here, P_p and y_i are total permeate pressure and MF of i on permeate side, respectively. Thus, Eq. (6) may be modified to Eq. (9).

$$J_i = \frac{P_i}{l}(x_i \gamma_i p_s - y_i P_p) \tag{9}$$

$$\text{or, } P_i = \frac{J_i l}{(f_i - y_i P_p)} \tag{9a}$$

Now, saturated VPs of i and j may be calculated using the Antoine equation. VP in the permeate side is too low to be considered and hence Eq. (9a) may be modified to Eq. (9b).

$$P_i = \frac{J_i l}{f_i} \tag{9b}$$

Intrinsic MS, α_{mem} may be obtained from the ratio of permeabilities using Eq. (10).

$$\alpha_{mem} = \frac{P_i}{P_j} \tag{10}$$

1-3. Diffusion Coefficient (DC)

In a binary system with a nonporous dense membrane, pervaporative flux (J_i) of i can be described by Fick's first law using Eq. (11) [32].

$$J_i = -\left(\frac{\rho_m D_i}{1 - W_{im}}\right)\frac{dW_{im}}{dl} \tag{11}$$

For very small W_{im}, the above equation reduces to Eq. (12).

$$J_i = -\rho_m D_i \frac{dW_{im}}{dl} \tag{12}$$

However, DC depends on the concentration of permeating components in membrane and their mutual coupling effect. DCs of i and j can be obtained using Eqs. (13) and (14), respectively [32].

$$D_i = D_{i0}\exp(W_{im} + \beta W_{jm}) \tag{13}$$

$$D_j = D_{j0}\exp(W_{jm} + \gamma W_{im}) \tag{14}$$

Substituting Eq. (13) in Eq. (12) results in Eq. (15).

$$J_i = -\rho_m D_{i0}\exp(W_{im} + \beta W_{jm})\frac{dW_{im}}{dl} \tag{15}$$

TF of i through the membrane was obtained via integrating Eq. (15) over the membrane thickness (Eq. (16)).

$$\int_0^L J_i dl = -\rho_m D_{i0} \int_{W_{imf}}^{W_{imp}} \exp(W_{im} + \beta W_{jm}) dW_{im} \tag{16}$$

For the present system, both THF and water will plasticize the membrane. Ignoring very low concentration of the permeating component on the downstream side, Eq. (16) reduces to Eqs. (17) and (18), respectively, for components i and j.

$$J_i = \frac{D_{i0}\rho_m}{L}[\exp(W_{im} + \beta W_{jm}) - 1] \tag{17}$$

$$J_j = \frac{D_{j0}\rho_m}{L}[\exp(W_{jm} + \gamma W_{im}) - 1] \tag{18}$$

From permeation data, J_i and J_j are obtained and from the sorption experiments, W_{im} and W_{jm} can be calculated. Thus, by a linear regression of the last two equations, DCs at different feed concentrations can be determined.

1-4. Measurement of Crosslink Densities (CDs)

Uncrosslinked NR membranes dissolve in hydrocarbon solvents, like toluene, pyridine, THF etc., depending on the closeness of their mutual solubility parameters. However, if the extent of crosslinking is very high, it can only swell to some extent without dissolution. For a given degree of CD, a better solvent will give higher degree of swelling. This relationship is quantitatively expressed by the Flory-Rehner Eq. (23) [24].

$$v = \frac{1}{V_s}\left[\frac{\ln(1 - v_r) + v_r + \chi_{ip} v_r^2}{\frac{1}{2}v_r - v_r^{1/3}}\right] \tag{23}$$

Here, v, V_s, v_r and χ are CD, molecular volume, VF and IP, respectively. CD by physical method is determined from the well-known equation (Eq. (24)) of kinetic theory of elasticity in its simplest form [24].

$$\sigma = RTv\left(\lambda' - \frac{1}{\lambda'^2}\right) \tag{24}$$

Here, σ is the stress to extend the crosslink rubber sample to extension ratio λ', R is the gas constant, T is the absolute temperature, v is the number of crosslinks in 1 cm^3.

2. Materials

NR of grade ribbed smoked sheets 3 (i.e. RSS3) and CBF of grade N330 (iodine no.=83.5 g Kg^{-1}, density=374 Kg m^{-3}, nitrogen sur-

face area=77.33 sqm g^{-1} and pH=7.12), were collected by PCBL (West Bengal, India). ZDC, sulfur powder and THF were purchased from Merck (Merck specialties private limited, India).

3. Preparation of Thin PV Membranes from Rubber-filler Dispersion

To prepare rubber-filler dispersion, NR was masticated by swelling it in toluene for 30 h. Varying proportions (8, 12 and 24 wt% of rubber) of CBFs were then added in portions with constant mechanical stirring to prepare a homogeneous dispersion. Sulfur (crosslinker, 4.91 wt% of rubber) and ZDC (accelerator, 4.86 wt% of rubber) were thereafter added to this dispersion with constant stirring for another 8 h. The resultant dispersion was then cast and kept overnight to dry under normal atmospheric conditions followed by crosslinking in a muffle furnace at 110 °C for 40 mins. The cured membrane was subsequently cooled by immersing the glass plate in cold water followed by peeling out from it. Thickness of the membrane was then measured with a thickness gauge at different regions. The average thickness of membrane used appeared to be 50±0.55 mm.

4. Vulcanization of Rubber Membranes

To make elastomers more useful, a chemical reaction, known as vulcanization or curing, was carried out to obtain crosslinked rubber chains. Vulcanized elastomers were found to have reversible elastic behavior under strain. Intramolecular bond in rubber moieties are generated by mono-, poly- and cyclic-sulfidic linkages during sulfur crosslinking, of which poly-sulfidic linkages give free mobility of chain segments. The movement of individual chain with respect to any stress, like pressure differential in PV, depends on the length of the bridge links of C-S_x-C (polythioether crosslinking). Higher the value of 'x', the easier it is for the chains to move [24,33]. On the other hand, maximum restriction in the rubber matrix is observed when crosslinking is achieved through much stronger and rigid mono-sulfidic linkages. Based upon the A/S ratios, vulcanization can be conventional (CV, A/S=0.1-0.6), semi-efficient (SEV, A/S=0.7-2.5) or efficient (EV, A/S=2.5-12.0). Open cure of rubber in conventional compression molding at a definite pressure and temperature could not be carried out for these too thin PV membranes. Consequently, membranes were cured at optimum cure temperature by incorporating cast rubber film in hot-air-oven without any pressure. In an open cure of rubber without pressure, rather higher doses of A/S are generally used. Thus, in the present work, A/S doses were fixed at 4.86/4.91 wt% of NR for SEV.

5. Accelerators in Rubber Vulcanization

As vulcanization is a kinetically slow process, accelerators are generally used to decrease the curing time at much lower temperature to obtain maximum extent of mono- and bi-sulfidic crosslinking. Early in the 20th century, several inorganic oxides were mainly used to speed up sulfur vulcanization at high temperature. Presently, organic substances are mostly used in small proportions to make it more productive and economical. Currently available accelerators are classified in several categories based on the difference in curing speeds, like slow-, medium-, semi-ultra- and ultra-accelerators, containing several chemical units (guanidines, thiazoles, sulphenamides, dithiocarbamates, thiuramsulphides, xanthates and aldehyde amines). Though NR contains unsaturation in its structure, an ultra-accelerator should be used at high temperature for better curing at convenient rates. ZDC, an ultra-accelerator, was used in the vulcanization of NR at 110 °C, having optimum curing time of 30 mins. ZDC has been reported to produce lower extent of poly-sulfidic bridges, in which the bridge length can be varied by varying the A/S ratios [24]. To obtain the minimum swelling after the attainment of equilibrium, rubber cured at 15 mins, 30 mins, 1 hr, 2 hrs, 3 hrs and 5 hrs and 10 hrs was immersed in THF.

6. Choice of Filler for Membrane Property/Performance Variations in PV

Fillers are added to elastomers to replace the use of expensive binders for improving important mechanical properties, like TS, EAB, modulus, abrasion resistance and tear strength. CBF, a colloidal form of elemental carbon is produced by partial combustion of oil or natural gases. The reinforcement power of CBF can be explained by the filler-polymer interface model, which states that the interface consists of two layers, glassy layer (~2 nm) and sticky layer (~3-8 nm). Glassy layer restricts chain mobility and increases stresses at small strains, whereas sticky layer extends from the glassy layer into the polymer and contributes an increase in stress at larger extensions [34]. When CBF is introduced into the rubber matrix, van der Waals force of attraction as well as covalent interactions prevail between the functional groups of CBF surface and rubber matrix. Depending on the energy site distributions of primary particle microstructures, which has dominant importance in controlling the surface activity of CBF particles, phase bonding and interparticle/interaggregate interactions are found to vary. As shown in Fig. 1(a), energy sites are of four different kinds, graphitic planes (1), amorphous carbon (2), crystallite edges (3) and slit shaped cavities (4) [35]. Relative energy/population of 1, 2, 3, and 4 in CBF of N330 grade is 16 kJ mol^{-1}/84%, 20 kJ mol^{-1}/7%, 25 kJ mol^{-1}/7% and

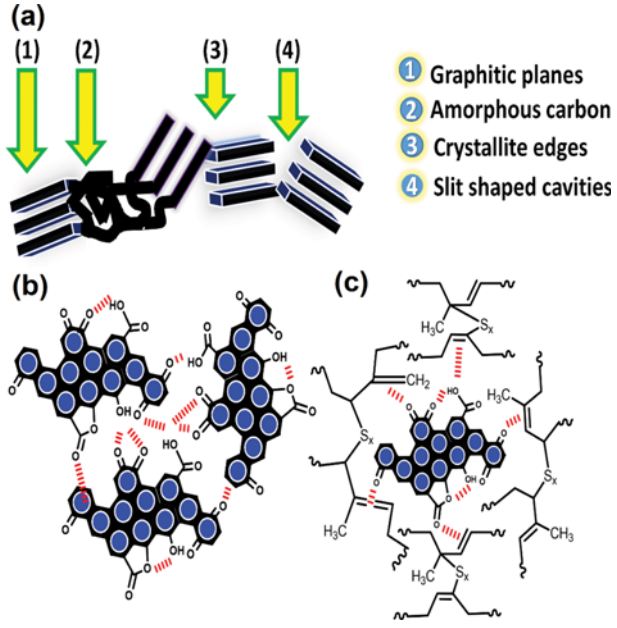

Fig. 1. Attribution of adsorption sites (a), agglomeration of CB particles in rubber matrix via physical/chemical interactions (b) and schematic representation of interactions between CBF and rubber chains (c).

30 kJ mol^{-1}/2%, respectively [36]. The relation between reinforcing strength of fillers and interaction strength with rubber matrix depends on the primary particle size of fillers, which decreases with high energy sites and becomes completely absent during graphitization. The prevalent attractive interaction between CBF and organic portion (Fig. 1(b)) depends on oxygen/heteroatom content and charge density of graphene layers. Several oxygen containing functional groups of CBF (quinone type carbonyl, phenolic hydroxyl, carboxyl, lactone, ether etc.) are either acidic or basic. Basic surface groups have an important role in several carbon utilization processes. Variation of the numbers of acidic (lactol, lactone, phenol and carboxyl) or basic (pyrones, chromenes and ketones) functional groups on the surface of CBF largely influences the electron cloud density of graphene layers and hence hydrophobic interactions [37]. Incorporation of CBF into the rubber matrix generates covalent and/or van der Waals force of interactions between functional groups of CBF and rubber matrix (Fig. 1(c)) for the reinforcement of rubbers. The variation of particle size of CBF from 10-500 nm largely influences the reinforcing properties of the elastomers, as it is established that lower the particle size, higher will be the reinforcement capacity. In fact, CBF of particle size 1,000-5,000 nm displays small reinforcement, whereas 500-1,000 nm and lower than 500 nm exhibits medium and strongest reinforcement strength, respectively [38]. Therefore, CBF of average particle size 30-45 nm was used in the present study.

7. Characterization of the Membranes

NRSEV membranes were characterized by measuring TS, EAB and modulus through Lloyd-UTM, England as per ASTM D 882-97 for polymeric film; field emission scanning electron microscope (FESEM) and energy dispersive X-ray (EDX) using JEOL JSM-7600F having resolution of 1 nm at 15 KV and 1.5 nm at 1 KV with the scanning voltage of 100 V to 30 KV; atomic force microscopy (AFM) via VEECO digital multimode nanoscope-IIIa, taping mode at the scanning rate of 2.001 Hz having scan size 5 mm; X-ray diffraction (XRD) by X'Pert PRO, made by PANalytical B.V., The Netherlands using Ni-filtered Cu K_α radiation (λ=1.5418 Å), scanning rate of 2θ=0.005°/s and angle of diffraction was varied from 2-72°; thermogravimetric analysis (TGA) using Pyris6 TGA, Netherlands in nitrogen atmosphere with flow rate of 20.0 cm^3/min at the scanning rate of 10 °C/min at 30-700 °C; fourier transform infrared (FTIR) spectroscopy through Spectrum-2, Singapore using a thin film in the range of 4,000 to 400 cm^{-1}) and differential scanning calorimetry (DSC) via Pyris6 DSC, The Netherlands in N_2 atmosphere with flow rate of 20.0 cm^3 min^{-1} at 30-442 °C. All graphical analyses were carried out using Origin 9.0 software. Software based image analysis on SEM photomicrographs was conducted by ImageJ, NIH, USA. RSM was carried out by using Design Expert 7.0.0 software.

8. Isothermal Sorption Study

To carry out sorption studies, different known concentrations of THF-water mixtures were prepared and membranes of known weights (1.00 g) were immersed within it. These were allowed to attain equilibrium for about four days at 35 °C. The samples were weighed periodically until constant weight was obtained and then taken out from solutions. The increase in weight due to immersion defined the total amount of THF and water sorped by membranes. After evaluating total sorption (TSP), the thick membranes were placed in a 100 cm^3 conical flask, maintained under constant temperature, accompanied by cold trap, which was further immersed in liquid N_2 as well as vacuum pump, connected in series (Fig. 2(a)). The sorped sample released vapor when heated under vacuum. This vapor was condensed in the cold trap, submerged in liquid N_2. Composition of this liquefied vapor, which gave the amount of THF sorped by membranes, was analyzed with a refractometer. Sorption selectivity (SS) of membrane (α_S) for THF could be calculated from the weight of total sorption and corresponding THF content [23].

$$\alpha_{S(i)} = \frac{y_{mi}/y_{mj}}{x_{fi}/x_{fj}} \tag{25}$$

Here, y_{mi}/x_{fi} denotes concentration of i in membrane/feed.

9. Pervaporation Experiment

PV experiments were performed in an isothermal batch stirred cell by circulating constant temperature water around the jacket of it, having an effective membrane area (A) and volume of the feed compartment as 19.00 cm^2 and 200.0 cm^3, respectively, and maintained at 1 torr by liquid Hg column method using a manometer with adaptable downstream pressure (Fig. 2(b)) [39]. The feed section of PV cell contained a stirrer and thermometer to ensure suitable mixing of liquid feed to eliminate either concentration or tem-

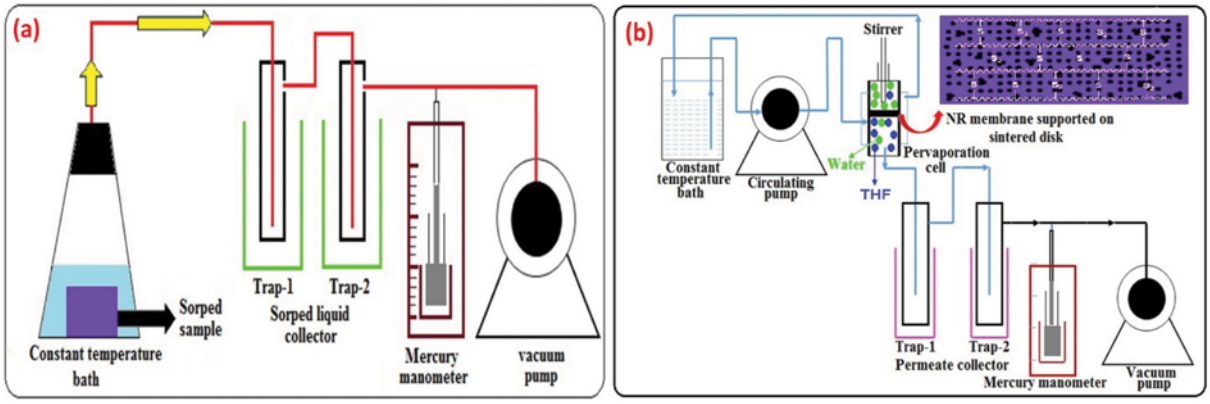

Fig. 2. Experimental setup for sorption (a) and pervaporation (b).

perature gradient. A sintered disk was placed at the center of the PV cell to hold the membrane. The upper part of this contained membrane, followed by feed mixture at 1 atm, whereas the lower part was made almost vacuum with the help of a vacuum pump. The feed mixture in contact with membrane was permitted to equilibrate for ~6 h for the first experiment followed by 4 h for subsequent experiments with varying feed compositions at different temperature. Permeate was condensed and collected in traps wrapped up by liquid N_2. Permeation flux (J) was calculated from the ratio of the amount of total permeates (W) to the product of time (t) of experiment and area of the membrane (A) by Eq. (26).

$$J = \frac{W}{At} \tag{26}$$

The corresponding THF content of permeate was estimated using a refractometer at 35 °C. SF of THF (α_{THF}) for all the membranes were evaluated using Eq. (27).

$$\alpha_i = \frac{y_i/y_j}{x_i/x_j} \tag{27}$$

Here, y_i/x_i are weight fractions of *i* in permeate/feed.

10. Design of Experiments

RSM is a widely used statistical method for modelling and analysis of responses of any experiment by performing minimum number of studies [40]. Optimization is mainly carried out by three steps, performing statistically designed experiments, estimation of the coefficients in a mathematical model and predicting the responses and examining adequacy of the model [41]. Central composite design (CCD), a standard RSM design, was applied to optimize three independent experimental conditions (temperature of experiment (X_1), wt% of THF in feed (X_2) and wt% of filler loading (X_3)) to understand their mere and interactive effect on two responses, TF and SF. Generally, CCD consists of 2^n factorial runs, 2n axial runs and n_c central runs [42]. The central points are utilized to evaluate experimental error and reproducibility of experimental data. The designed experiments were carried out in randomized form to minimize the effects of uncontrolled factors [42,43]. Responses were analyzed and correlated with input variables for optimization based on the following empirical second order polynomial equation.

$$Y = \beta_0 + \sum_{i=1}^{3}\beta_i X_i + \sum_{i=1}^{3}\beta_{ii} X_i^2 + \sum_{i=1}^{3}\sum_{j=1}^{2}\beta_{ij} X_i X_j \tag{28}$$

Here, Y, β_0, β_i, β_{ii} and β_{ij} represent the predicted response, constant, linear, quadratic and interaction coefficient(s), respectively. To justify the significance and adequacy of the predicted model by analysis of variance (ANOVA), independent experimental conditions were taken as coded variables in the range of −1 (minimum) to +1 (maximum). Data obtained from experiments were fitted to Eq. (28) for obtaining regression coefficients (R^2). The minimum (−1) and maximum (+1) levels taken for the independent variables (wt% of accelerator (P)/sulfur (Q) and $X_1/X_2/X_3$) for optimization of TS/EAB and TF/SF (Table 1). The primary objective of first optimization was to ensure the optimum A/S ratio for producing NR membrane having the best balance of TS/EAB. Again, in the second case, maximum THF recovery from THF-water system was ensured by the establishment of optimum conditions for maximum SF of NRSEV membranes. The following criteria were em-

Table 1. Maximum and minimum data ranges for the parameters to be optimized using two steps RSM

Parameters	Maximum range (−1)	Minimum range (+1)
X_1	35 °C	55 °C
X_2	2.44	7.34
X_3	0	24
P	2 wt%	8 wt%
Q	3 wt%	6 wt%

Table 2. Physical properties of membranes

Membrane/ Thickness (μm)	CD×10^4 (mol cm^{-3}) (Chemical method)	CD (MPa) (Physical method)	Modulus/ % elongation (MPa)	TS (MPa)/ EAB (%)	Ref.
PDMS/33[a]	-	-	-	1.82/94.8	44
PDMS/85[a]	-	-	-	1.91/120.2	44
PDMS/189[a]	-	-	-	1.97/198.9	44
PDMS/285[a]	-	-	-	2.12/250.7	44
EPDM/-[b]	-	-	1.4/200	2.40/388.5	45
EPDM0/50[b]	4.89	6.45	0.34/100	4.46/750.0	31
EPDM2/50[b]	7.20	10.65	0.48/100	6.24/337.3	31
EPDM4/50[b]	8.83	13.56	0.57/100	7.15/245.2	31
EPDM6/50[b]	9.30	14.56	0.62/100	7.89/172.1	31
NRSEV0/50±0.55	3.06	4.80	0.44/100	5.66/520	TS[#]
NRSEV8/50±0.55	3.57	5.40	0.98/100	11.35/500	TS[#]
NRSEV12/50±0.55	3.82	5.65	1.54/100	14.77/486	TS[#]
NRSEV24/50±0.55	4.25	5.93	1.69/100	15.25/424	TS[#]

[a]Polydimethylsiloxane

[b]Ethylene polypropylene diene monomer

[#]This study

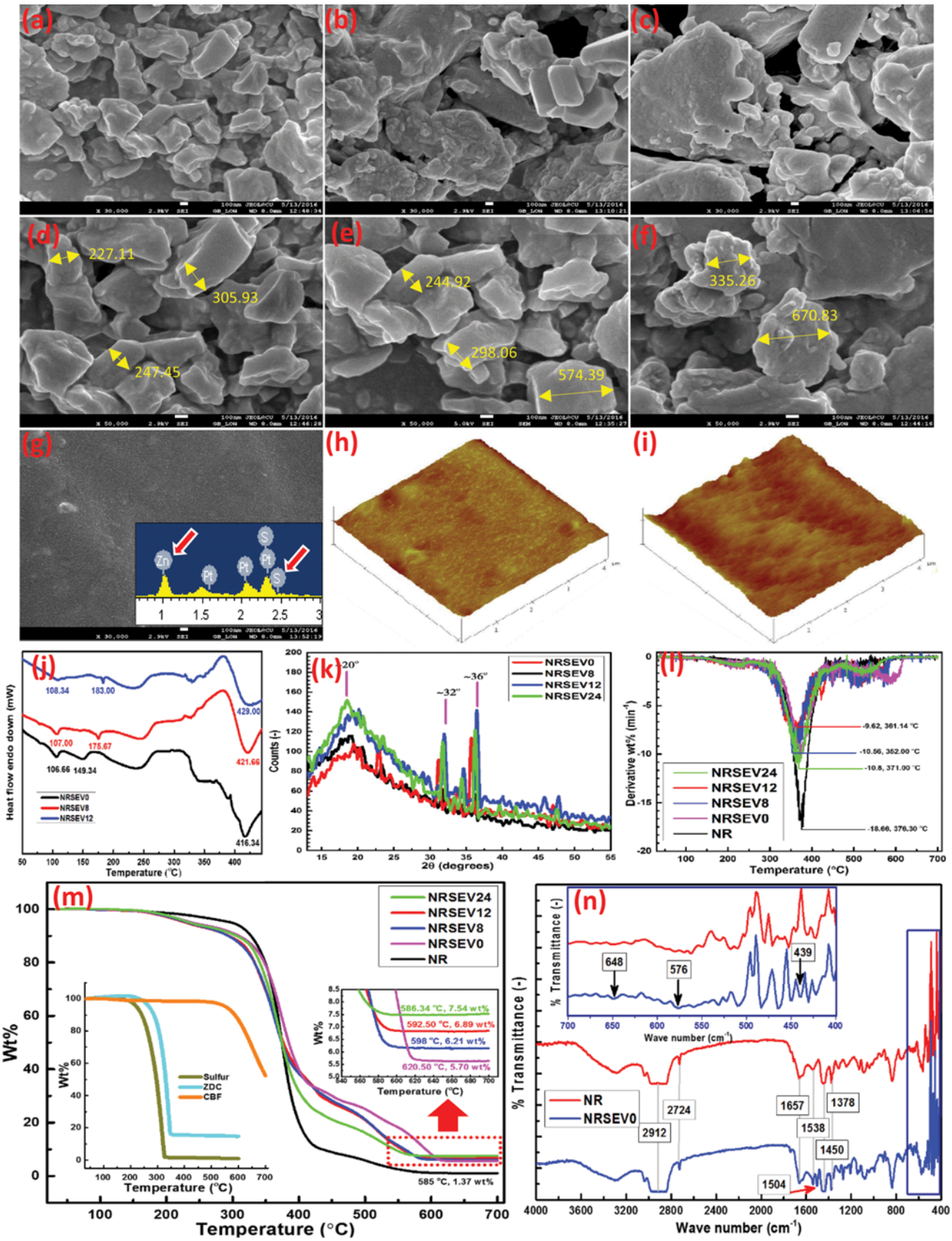

Fig. 3. FESEM of NRSEV8/30kX (a), NRSEV12/30kX (b), NRSEV24/30kX (c), NRSEV8/50kX (d), NRSEV12/50kX (e), NRSEV24/50kX (f), NRSEV0/30kX (g), EDX of NRSEV0 (inset of g), AFM of NRSEV0 (h), NRSEV12 (i), DSC (j), XRD (k), DTG (l), TGA (m), TGA of S/ZDC/CBNF (inset of m) and FTIR (n).

ployed in the numerical optimization section of the software: X_1, X_2, X_3, P, Q and TF: 'in range' and SF: 'maximize'.

RESULTS AND DISCUSSION

1. Variation of Mechanical Strength and Crosslink Densities (CDs)

The variation of TS, EAB and modulus of filled and unfilled NRSEV membranes is given in Table 2. With the rise in physico-chemical interactions via insertion of surface reinforcing filler, chain flexibility of rubber moieties was found to decrease that led to the inverse variation of TS/modulus and EAB [33]. However, TS was also increased with the rise in filler at the cost of EAB. Thus, these membranes showed good balance of TS and EAB as required in PV.

Chemical and physical CDs of NRSEV membranes were com-

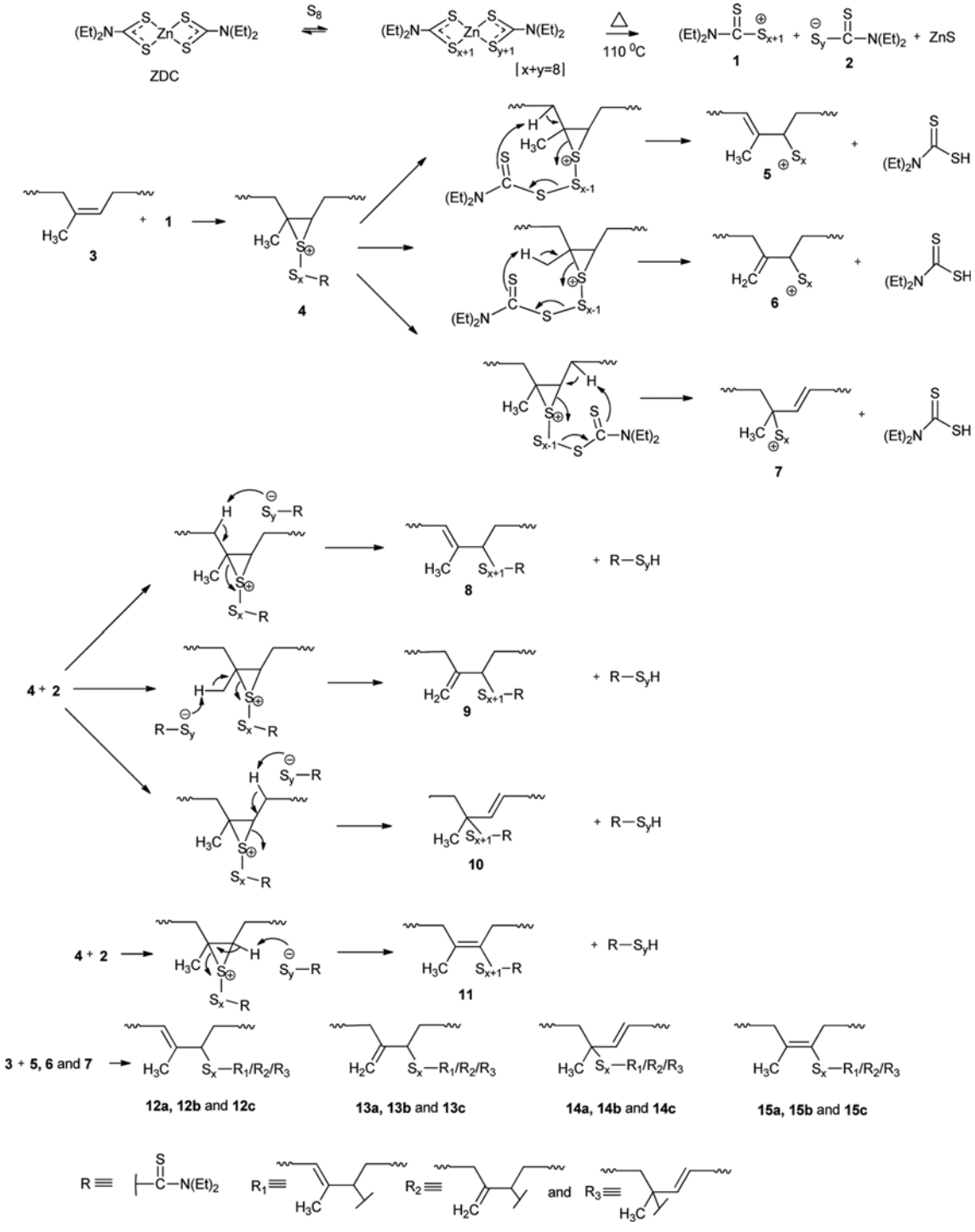

Scheme 1. Sulfur vulcanization through ionic path.

parable with other reported rubber membranes (Table 2). From these values, it appeared that CDs of the rubber membranes increased with filler loading due to the incorporation of high structure fillers in the voids of rubber matrix. The increase in CDs was due to the increase in physical crosslinking from NRSEV8 to NRSEV24 by the weak van der Waals force of attraction between functional groups of CBF surface and rubber chains.

2. Field Emission Scanning Electron Microscope (FESEM) and Energy Dispersive X-ray (EDX)

FESEM at higher magnification (30 kX and 50 kX) was conducted to ensure the change in morphology due to the distribution of CBFs in membrane matrix. In fact, morphology coarsening was observed in the used membranes with the increasing amount of filler (Fig. 3(a)-(f)). However, featureless dense morphology in

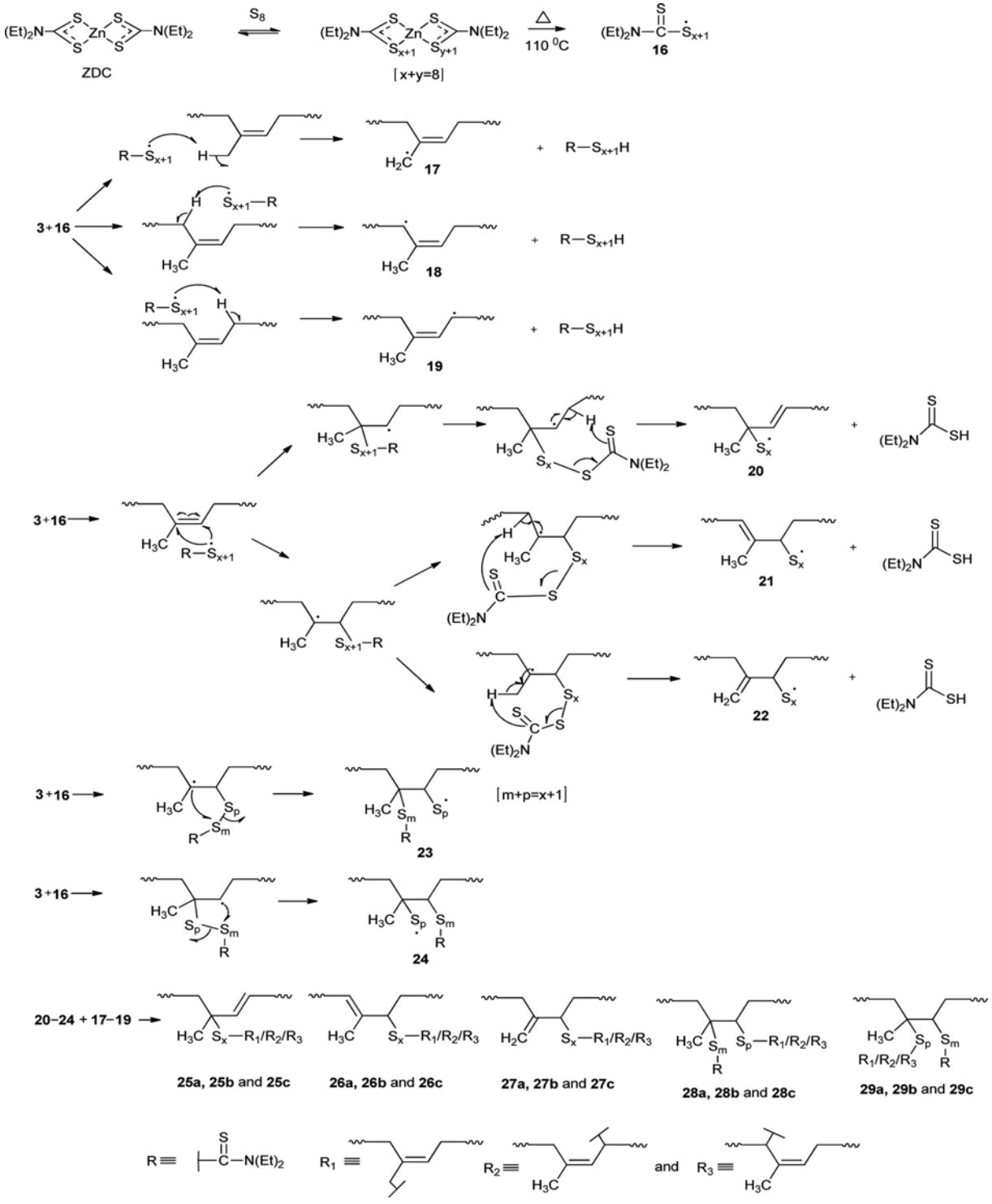

Scheme 2. Sulfur vulcanization through radical path.

unfilled NRSEV0 membrane was also observed due to close vicinity of rubber chains by bi- and poly-sulfidic crosslinking (Schemes 1 and 2) in accelerated sulfur vulcanization (Fig. 3(g)). Rough surface and uneven distribution of fillers were observed with the increasing amount of filler, due to strong filler-filler interaction, resulting agglomeration of particles in the composite matrix. In fact, particle agglomeration was confirmed by the increase in particle dimension (L/B ratio) of CBFs in the order of, 436.45 (nm)/239.16 (nm), 523.33 (nm)/336.25 (nm) and 843.47 (nm)/523.33 (nm) for NRSEV8, NRSEV12 and NRSEV24, respectively [31]. However, the use of 0.9898 weight ratio of A/S for SEV was also confirmed from the relative peak intensities of zinc and sulfur in the selected area of EDX spectra (inset of Fig. 3(g)).

3. Thermogravimetric (TGA), Differential Thermal Gravimetric (DTG) and Differential Scanning Calorimetric (DSC) Analyses

The TGA diagram (Fig. 3(m)) of elastomeric membranes shows two major weight loss regions (~1-89 wt% and ~89-98 wt% for NR but ~1-70 wt% and ~89-93 wt% for NRSEV0, NRSEV8, NRSEV12 and NRSEV24, respectively) along with the onset of degradation at around 170 °C (loss of ~1 wt%). Weight loss in the range 170 °C to 200 °C for all the membranes was due to the removal of volatile components (e.g., stearic acid and adsorbed moisture) [46]. The first major region of weight loss was ascribed to the degradation of NR backbone (poly-isoprene) into gaseous products, whereas in the second stage of degradation [47], weight loss was associated with the scission of NRSEV and conjugated polyene (which was left after the first stage of degradation) [48]. However, the maximum degradation temperature was found to vary within 585-620.5 °C for the used vulcanized and composite membranes (From Fig. 3(m), confirmed the final decomposition of occluded rubber moieties within filler aggregates. The amount of residues for sulfur, ZDC and CBF were 1.14, 14.7 and 52 wt%, respectively (inset of Fig. 3(m)). Therefore, the amount of percentage residue for raw NR (1.37 wt%) was exceptionally low in comparison to the filled and crosslinked membranes (5.70-7.54 wt%), signifying the presence of S, ZDC and CBF residues. With increasing filler loading, the residue formation was found to increase (5.62, 6.09, 6.90 and 7.6 wt% for NRSEV0, NRSEV8, NRSEV12 and NRSEV24, respectively), indicating the increasing amount of CBF in the membranes. Complete degradation of polymer backbone, within 585-620.5 °C, was ensured from the increasing amount of residue formation with increasing amount of CBF (also ZDC and sulfur) in the composite membrane as beyond 620.5 °C, only CBF, ZDC and sulfur survived. As observed in DTG (Fig. 3(*l*)) diagram, the maximum rate of thermal decomposition/maximum degradation temperature for NRSEV24, NRSEV12, NRSEV8, NRSEV0 and NR were −10.8 wt%/371 °C, −9.62 wt%/361.14 °C, −10.56 wt%/352 °C, −10.07 wt%/379.4 °C and −18.66 wt%/376.3 °C, respectively, which explained the minimum thermal stability of raw NR membrane at comparable maximum decomposition temperature. The thermal stability was found to increase remarkably with chemical crosslinking (from NR to NRSEV membranes) but did not vary significantly with physical crosslinking (with increasing CBF loading from 0-24 wt%), signifying the fact that chemical crosslinking affected the thermal properties more than filler incorporation. From Fig. 3(j), several endothermic heat losses were observed in ranges, like 106.66-108.3 °C, 149.34-183.00 °C, 416.34-429.00 °C etc. In fact, the appearance of crystalline melting temperature (T_m) was found to increase from 149.34 to 183.00 °C, owing to better physicochemical crosslinking by higher amounts of surface reinforcing fillers. However, a portion of occluded rubber, surrounded by CBF aggregates, showed better thermal stability, even at much higher temperature ranges (416.34-429.00 °C or higher ranges). Altogether, thermal stability of used membranes, as reflected from TGA and DSC analyses, was found to increase significantly with crosslinking and filler loading.

4. X-ray Diffraction (XRD)

From characteristic XRD pattern of four filled and crosslinked membranes, considerable variation in the physicochemical interactions were obtained due to the variation of wt% of CBF (Fig. 3(k)). Incorporation of filler resulted in an increase in physical crosslinking, TS/modulus and hence physicochemical interactions due to filling of voids in the rubber matrix. Symbolic peak intensities of XRD at the specified 2θs (~20°), were decreased in the order, NRSEV24> NRSEV12>NRSEV8>NRSEV0, signifying decrease in physicochemical interactions by the same order [31]. Similar change in physicochemical interactions was also observed in TGA and DTG diagrams. The prevalent fillers of high surface area resulted an increase in physicochemical interactions due to increase in TS, modulus and physical and chemical crosslink densities. Miller distances (d_{100}~2.45 Å, n=1; d_{200}~3.80 Å, n=2), determined from sharp symbolic peak intensity of XRD in the proximity of 2θ~31°/36° in all composite membranes, were almost identical to the single layer of graphene [49]. Unfilled NRSEV0 contributed lowest physicochemical interactions due to the absence of physical crosslinking, as evident from minimum peak intensity of XRD.

5. Atomic Force Microscopy (AFM)

AFM was also used to determine the change in rubber surface morphology of composite membranes by filler microdispersion. It was found that high structure CBFs protruded in the rough surface of elastomer and well dispersed without agglomeration [50]. In fact, morphology of filled membranes also looked different from the unfilled matrix. However, in filled membranes, the rough surface at micrometer level was observed, whereas unfilled but crosslinked membrane showed relatively smoother surface (Fig. 3(h)-(i)).

6. Fourier Transform Infrared Spectroscopy (FTIR) Analysis

FTIR spectra (Fig. 3(n)) of NR and NRSEV0 membranes showed characteristic peaks at 2,912/2,724, 1,657/1,538, 1,450 and 1,378 cm^{-1} for C-H unsymmetrical/symmetrical stretching vibrations of methylene (-CH_2-) group in the saturated hydrocarbon backbone, C=C stretching, -CH_2- scissoring and C-H symmetrical bending vibration of methyl groups, respectively [24]. However, symbolic peaks in the range 700-600 and 500-400 cm^{-1} represented the appearance of C-S-C/C-S and S-S bonds, respectively [50]. More importantly, NRSEV0 membrane also showed distinct peaks of C-S and S-S bonds at 648/576 and 439 cm^{-1} as a result of sulfur crosslinking [24,51]. However, C-S band appeared at a frequency higher than S-S band due to different extents of S-S (B.E=57 kcal $mole^{-1}$) and C-S (B.E=65 kcal $mole^{-1}$) bond stabilities. In fact, vulcanization at double bonds was also reflected by the symbolic appearance

of a new band at 1,504 cm^{-1} and decrease in C=C peak intensities at 1,657 and 1,538 cm^{-1}. Indeed, chemical crosslinking decreased the population of prevalent double bonds, and thus fewer double bonds were available in crosslinked membranes for free physical interaction with the functional groups of CBFs. In this regard, it is important to note that FTIR spectra of the filled membranes were not carried out as CBF blocked the passage of IR radiation through the composite membranes.

7. Variation of Interaction Parameters (IPs), Total Sorption (TSP), Sorption Selectivity (SS) and State-I/II/III Activity Coefficients (ACs) of THF (i) and Water (j) with Feed Concentration of THF

IP between solvents in feed (χ_{ij}^{f}) was determined using Eq. (1a). To determine IPs of solvents with membrane (χ_{ij}^{m}), χ_{ij}^{f} was first plotted with volume fractions (V_i) of THF in feed to obtain a polynomial trend line (χ_{ij}^{m}=30.4675u_i^2–7.7673u_i+7.0025) having R^2 closest to unity. The variation in IPs of solvents with feed concentration of THF in feed and membranes (both unfilled and filled) were shown in Fig. 4(a). Higher the value of IP, the lower will be the mutual interaction between solvents. However, with the increase in feed concentration, IP between THF and water increased in membrane phase, whereas IP was found to decrease in the feed side. From Fig. 4(a), we also observed that membrane phase IPs were much higher than feed IPs. Thus, mutual interaction between solvents in feed was higher than their interactions in membrane, resulting in sorption of solvents by these membranes. However, the mutual interaction between two solvents during sorption was decreased relatively in membrane phase with the increasing feed concentration. This indicated that THF recovery became easier with increasing concentration owing to plasticization of the organophilic rubber membranes. Initially, increase in IPs of components from NRSEV0 to NRSEV12, followed by its decrease from NRSEV12 to NRSEV24, indicated better THF recovery with increasing filler loading up to 12 wt%. Thus, no further study was carried out beyond 24 wt% of filler incorporation. Hydrophobic CBF enhanced organoselectivity of NRSEV membranes. Again, with increasing filler loading, χ_{ip}/χ_{jp} in membranes were found to follow the order, NRSEV24 (0.5046/0.8969)>NRSEV12 (0.5040/0.8506)>NRSEV8 (0.5032/0.7963)>NRSEV0 (0.5025/0.7350).

It was observed from Fig. 4(b) that TSP and SS showed an opposite trend with increasing feed concentration of THF. In fact, with increasing concentration, more THF was adsorbed by the organophilic membranes. However, the feed concentration of THF was insufficient for dissolving used membranes except loosening of the polymeric chains, which resulted the higher permeation. TSP of the unfilled membrane was higher than CBF filled membranes, whereas SS was lower for unfilled membranes, possibly due to the inverse variation of increased physicochemical interactions and total sorption of these membranes. Actually, with increasing filler loading, enhanced physicochemical interactions caused filling of voids in the rubber network resulting in lower amount of TSP. However, the increased organophilicity of the rubber membranes by incor-

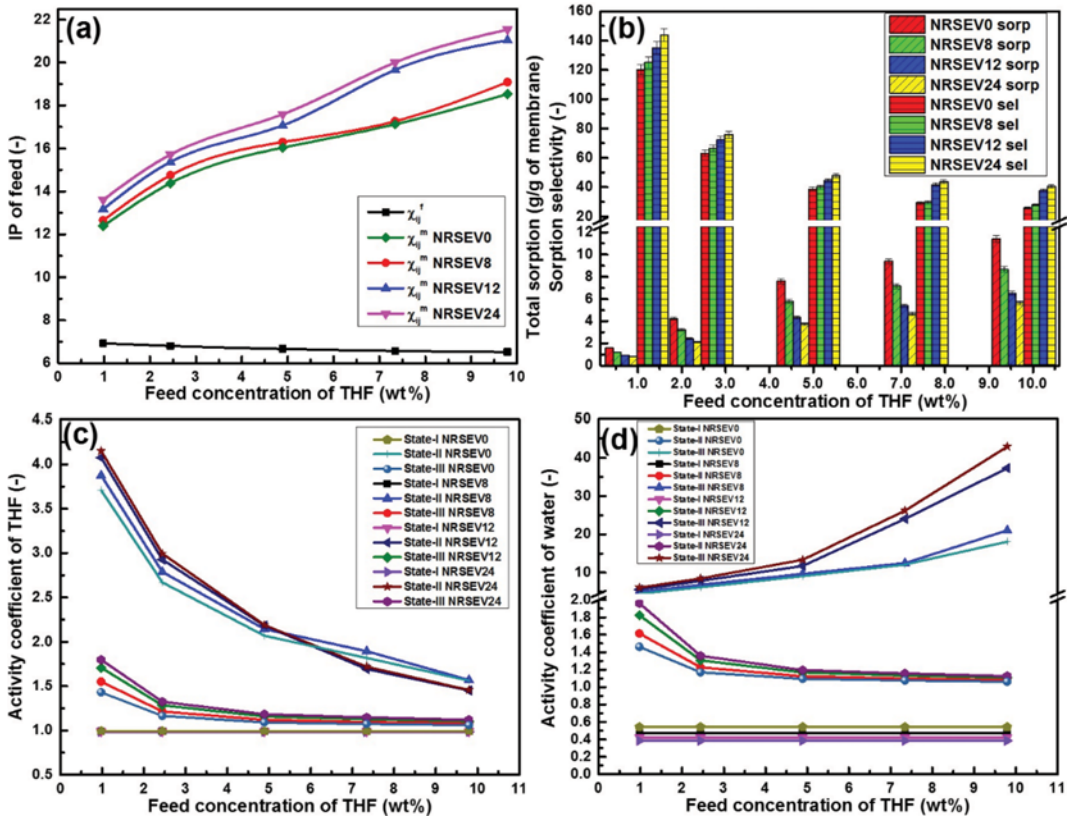

Fig. 4. Variation of interaction parameter (a), total sorption and sorption selectivity (b), state-I/II/III activity coefficients of THF (c) and water (d) with feed concentration of THF.

poration of CBF enhanced THF selectivity. In this regard, the opposite trend of TSP and SS with feed was also reported by Singha et al. [31]. All the experiments were repeated thrice and standard deviations (SD) of the obtained results were estimated to confirm reproducibility. SD variation within 2-4% of the mean value indicated fair reproducibility as well as high confidence limit of the results within a narrow confidence interval [24]. For 0.97 wt% THF in feed, TSP/SS of NRSEV24 membrane were found to be 0.79± 0.025 (g/g of membrane)/143.72±4.31.

The variation of activity coefficients of THF and water within NRSEV membranes with feed concentration is given in Fig. 4(c), (d), respectively. The preferential separation of one solvent from its binary mixture can be apprehended from the interactions of each liquid with membrane as well as with each other. A comprehensive approach to understand the coupling effect is to study the change in activity coefficient of each component in thermodynamic swelling process. This change can arise from two types of coupling, interaction of each component with membrane matrix and mutual interaction between components within the membrane. Separation of two miscible solvents by selective sorption can only be possible if the interaction of a particular solvent with membrane matrix predominates over mutual interaction with other solvent. To account for the contribution of coupling effect from activity coefficient of each component within membrane, three distinct curves of activity coefficients in different states were considered, state-I indicated the activity coefficient of pure (ideal) component within the membrane acting as a reference followed by state-II, describing the activity coefficient of component i in reference state to consider the interaction between individual component within membrane/membrane matrix and finally state-III activity coefficients, which illustrated the mutual interaction of both components within membrane in thermodynamic swelling process. The deviation between state-I and state-II illustrates the interaction between each component and the membrane matrix with the change in feed concentration, whereas state-II and state-III deviation indicates the contribution of the coupling effect between the two components within the membrane [31]. From Fig. 4(c), the deviation from state-I and state-II was higher than that of state-II and state-III at low feed concentration. This suggested that the interaction of THF with the membrane matrix was much higher than the mutual interaction with water, signifying higher possibility of THF recovery by such organophilic membranes [31]. Also, the deviation of state-I and state-II became smaller with the increasing amount of THF in feed, resulting in lower extent of THF sorption. High THF in feed caused loosening of membrane crosslinks, allowing segmental motion of rubber chains, and hence more water was permeated along with the THF. Thus, SF was found to decrease with increasing feed concentration of THF. It was also observed that the deviation of state-II and state-III became minimum for 24 wt% of filler loading, indicating least possibility of THF-water mutual interaction in comparison to other membranes, and hence maximum THF recovery was ensured for this composite membrane. However, from Fig. 4(c), the deviations of state-I and state-II and state-II and state-III were higher and lower for the CBF filled NRSEV membranes than the unfilled membrane, respectively, signifying better SF of the filled NRSEV membranes. As observed in Fig. 4(d), deviation of state-I

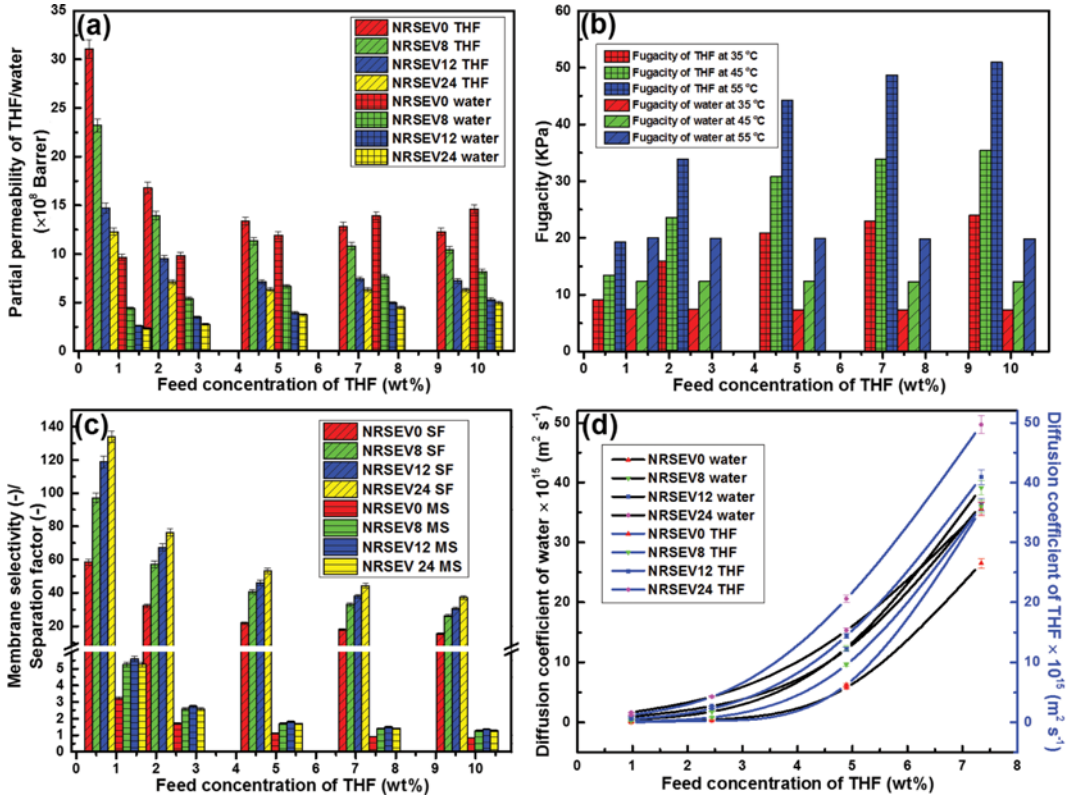

Fig. 5. Effect of feed concentration of THF on partial permeability (a), fugacity (b), MS/SF (c) and diffusion coefficient (d).

and state-II was much lower compared to state-II and state-III, signifying stronger mutual interaction of water with THF than composite membranes.

8. Effect of Feed Concentration of THF on Partial Permeabilities (PPs), Fugacities, Membrane Selectivities (MSs), Separation Factors (SFs) and Diffusion Coefficients (DCs)

The variation in PPs of THF and water with feed concentration of THF at 35 °C for unfilled and CBF filled NRSEV membranes is shown in Fig. 5(a). However, PPs of the membranes were calculated from membrane thickness, partial flux and vapor pressure (VP) difference of feed and permeate sides. All membranes showed higher PPs of THF than water over the entire concentration range of THF in feed. However, at low concentration, PP decreased with feed concentration up to around 5 wt% of THF which contrasted with the variation of partial THF flux. Conversely, water PPs showed hardly any variation with increasing THF amount for all the membranes. It was also observed that THF PPs decreased with filler loading and CBF filled NRSEV membranes were found to have lower THF PPs than the unfilled membrane, similar to what Singha et al. observed [31]. PPs of THF/water were found to vary from $(3.11\pm0.093)\times10^{-7}$ to $(1.23\pm0.037)\times10^{-7}$/$(0.97\pm0.029)\times10^{-7}$ to $(1.460.044)\times10^{-7}$ Barrer for NRSEV0 membrane with the rise in THF feed amount from 0.97 to 9.79 wt% in feed at 35 °C.

Intrinsic membrane property, like PP is related inversely to driving force of VP differential between feed and permeate sides and directly to flux. Thus, partial flux showing considerable variation with feed concentration might show a different trend with feed concentration in terms of driving force normalized PP or MS. The opposite trend of THF PP in comparison to THF flux as a function of feed concentration might be explained in terms of variation of

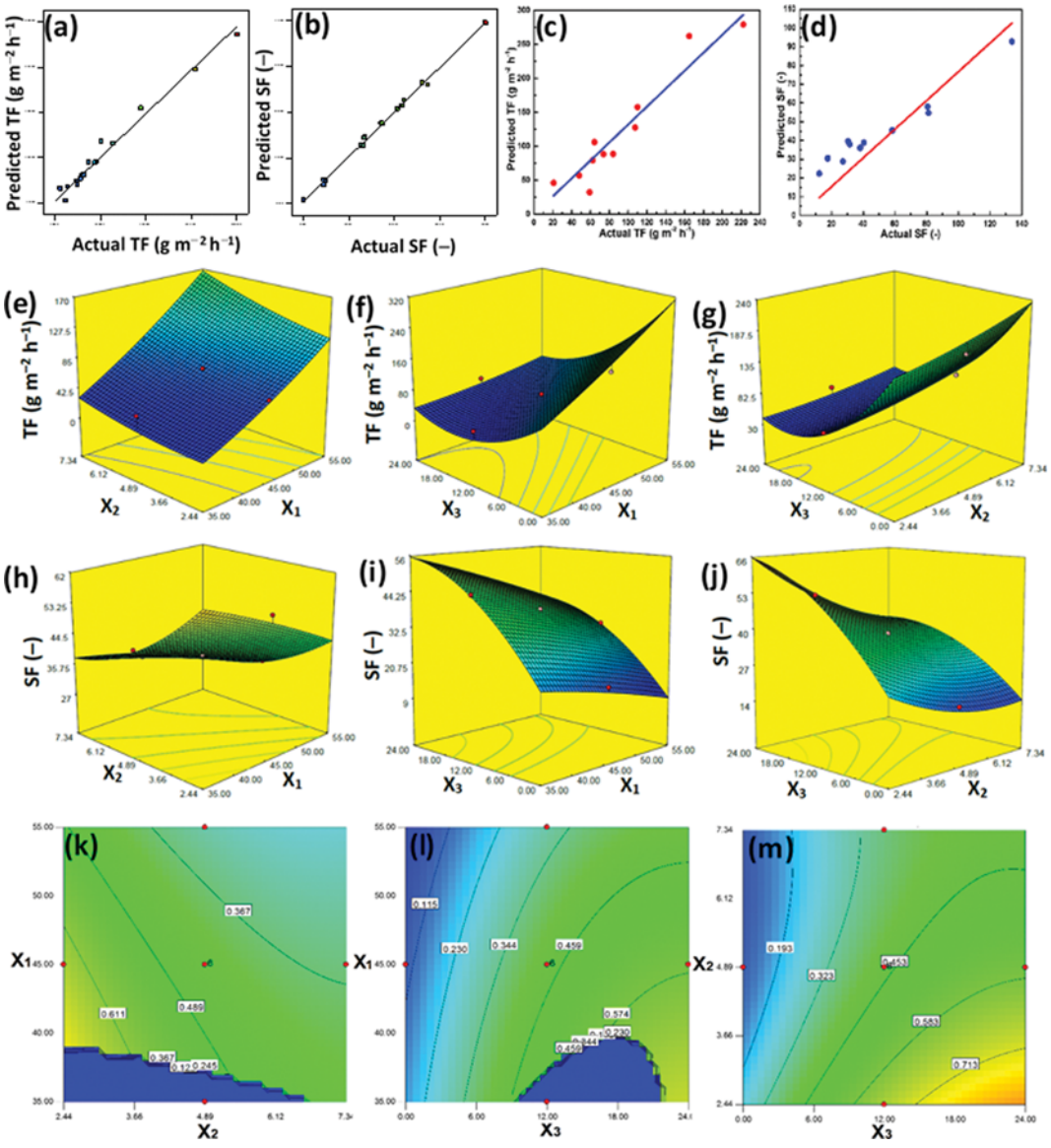

Fig. 6. Predicted vs. actual plot of TF (a)/SF (b), validation plot of TF (c)/SF (d), response surface plots: Effect of wt% of THF (X_2) and temperature (X_1) on TF/SF (e/h), effect of wt% of filler (X_3) and temperature (X_1) on TF/SF (f/i), effect of wt% of filler (X_3) and wt% of THF (X_2) on TF/SF (g/j) and desirability plots for optimization of maximum SF (k-m).

fugacity with feed concentration as shown in Fig. 5(b).

Comparing the plots of THF flux (Fig. 6(e), (g)) and THF PPs (Fig. 5(a)) as a function of feed, it was evident that, the rate of change in THF fugacity with feed THF concentration was much higher than that of partial flux. Thus, THF PP decreased with increasing feed concentration owing to higher increasing rate of THF fugacity (Fig. 5(b)). From Fig. 5(a), the marginal variation of water PPs in the entire range was ascribed to slight variation of water fugacity (Fig. 5(b)) and partial flux. At higher feed concentration of THF, loosening of membrane network occurred due to plasticization, which resulted in segmental motion of rubber chains and hence enhancement of THF PPs for organophilic rubber membranes. Similar results were also obtained with other rubber membranes [30]. Variation of intrinsic MS as well as SF with feed concentration of THF is shown in Fig. 5(c), where it is seen that all the elastomeric membranes had very high SF even at lower feed concentration. However, MS showed a marginal decrease with increase in concentration due to plasticization of the organoselective rubber membranes at higher feed concentration. From Fig. 5(a), PPs of THF was observed to drop more rapidly, whereas water PPs showed a very slow rate of fall with the increase in THF concentration. Thus, the ratio of these two followed a sharp decrease with increasing feed concentration. On the other hand, SF for THF was observed to decrease sharply with its feed concentration. From Fig. 5(c), it is also evident that both MS and SF increased with increasing filler loading, i.e., NRSEV0 showed lower MS and SF than filled membranes. With increasing amount of organophilic CBF, organoselectivity of rubber membranes was found to increase, resulting in more selective removal of THF. However, MS/SF of NRSEV24 membrane was found to decrease from 5.26±0.16/133.96±3.48 to 1.28± 0.04/37.2±1.19 with the rise in feed concentration from 0.97 to 9.79 wt% of THF in feed at 35 °C.

The variation of DCs of THF and water with feed concentration of THF for unfilled and CBF filled composite membranes was given in Fig. 5(d), in which DCs of THF were higher than water in the lower feed concentration. Also, DCs of both THF and water increased with feed concentration. According to solution-diffusion model, selective separation of liquids from their binary mixture through sorption generally occurs via sorption followed by diffusion and finally permeation. Sorption of components to the membrane is guided by the closeness of solubility parameters of membrane and component, whereas diffusion mainly depends on the porosity of dense membrane. In the present study, solubility parameters of used membranes, as calculated from Eq. (3), were 17.0055 $MPa^{0.5}$ (NRSEV0), 17.0003 $MPa^{0.5}$ (NRSEV8), 16.9946 $MPa^{0.5}$ (NRSEV12) and 16.9906 $MPa^{0.5}$ (NRSEV24). In fact, closeness of these solubility parameters with that of THF (19.2 $MPa^{0.5}$) signified larger interaction of THF with these membranes than water (48.0 $MPa^{0.5}$) [31]. Thus, membranes were predominantly organoselective and sorption of THF was higher than water. However, higher possibility of water diffusion and hence higher DCs of water through these dense membranes were expected owing to smaller kinetic diameter of water (0.265 nm) than THF (0.585 nm) [27]. Since sorption of THF was much higher than water, DCs was also higher, in spite of higher kinetic diameter. Additionally, DCs of THF was found to be higher for NRSEV0 membranes compared to NRSEV8, NRSEV12 and NRSEV24. In fact, DCs of both components were found to increase with filler loading. Indeed, with increasing amount of filler, plasticization was restricted due to higher physicochemical interactions even at higher feed concentration of THF, offering restricted permeation of both components. Since more sorption and hence diffusion signified greater separation, all the used NRSEV membranes showed high THF SF, justifying their organoselective nature. DCs of THF/water was observed to vary from $(0.07\pm0.002)\times10^{-15}/(0.02\pm0.0007)\times10^{-15}$ m^2 s^{-1} to $(26.53\pm0.796)\times10^{-15}/(35.54\pm1.066)\times10^{-15}$ m^2 s^{-1} with the rise in THF feed concentration from 0.97 to 9.79 wt% in feed at 35 °C.

9. Analysis of Mere and Interactive Effects of Variables on TS and EAB by RSM

Experimental design of RSM was implemented to obtain the optimum accelerator/sulfur weight ratio for vulcanization of NR (Table S1). This optimization was carried out by taking wt% of sulfur and accelerator as input variables using CCD model to obtain two responses (TS and EAB). CCD studies on TS and EAB evolved the following two quadratic equations.

$$R_{TS}=2.62082+1.87655P-0.26241Q+0.036667PQ-0.14243P^2-0.00750958Q^2 \quad (29)$$

$$R_{EAB}=365.51245-22.76724P+61.63793Q-2.72222PQ+0.8295P^2-3.34866Q^2 \quad (30)$$

Optimization of TS and EAB was performed by applying Eqs. (29) and (30) and the results obtained were given as ANOVA (Table S2). The response surface and optimization plots of TS and EAB were given in Fig. S2(a), (b) and Fig. S3(a), (b), respectively. The variation of TS and EAB with wt% of sulfur and accelerator was displayed in Fig. S2(a), (b), respectively. TS and EAB were observed to vary inversely with increasing A/S ratios [24]. As TS depends on the physicochemical interactions of rubber membrane, improvement of physicochemical interactions by incorporation of surface reinforcing filler caused an increase in TS. On the other hand, higher physicochemical interactions caused restriction towards chain mobility of rubber moieties resulting in a decrease in EAB. However, to develop mechanically strong and dimensionally stable NR membranes, a perfect balance of TS and EAB was essential [52]. This was achieved by optimizing TS and EAB using RSM to obtain optimum A/S ratio in vulcanization by performing thirteen (13) runs with nine (9) different membranes ranging from 2-8 wt% of accelerator and 3-6 wt% of sulfur. From Fig. S3(a), (b), the optimized values of input variables were found at 4.86/4.91 wt% of A/S (i.e. A/S= 0.9898) reflecting SEV type vulcanization [24]. Thus, semi-efficiently crosslinked and filled NR membranes were used for pervaporative removal of hazardous heterocyclic THF.

10. Analysis of Mere and Interactive Effects of Variables on Responses by RSM

CCD studies were carried out to establish the influence of three different parameters (X_1, X_2 and X_3) individually or collectively on the responses [53]. Independent variables (coded and real) and responses generated by the software are listed in the Table S3. The significance of each variable and their possible interactions were measured by ANOVA to determine R^2 between experimental and predicted data at 95% confidence level (Table 3). To understand

Table 3. ANOVA for SF/TF

Source	Sum of squares	df	Mean square	F value	P-value
Model	4350.06/137800.00	9/9	483.34/15307.48	354.46/55.64	<0.0001*/<0.0001*
X_1	541.40/36701.00	1/1	541.40/36701.00	397.03/133.41	<0.0001*/<0.0001*
X_2	971.02/3521.16	1/1	971.02/3521.16	712.10/12.80	<0.0001*/0.0050*
X_3	2479.75/60912.25	1/1	2479.75/60912.25	1818.52/221.42	<0.0001*/<0.0001*
X_1X_2	36.09/505.63	1/1	36.09/505.63	26.46/1.84	0.0004*/0.2050
X_1X_3	20.04/14622.42	1/1	20.04/14622.42	14.69/53.15	0.0033*/<0.0001*
X_2X_3	125.75/611.60	1/1	125.75/611.60	92.22/2.22	<0.0001*/0.1668
X_1^2	1.68/120.06	1/1	1.68/120.06	1.23/0.44	0.2928/0.5238
X_2^2	56.53/76.30	1/1	56.53/76.30	41.46/0.28	<0.0001*/0.6099
X_3^2	138.01/8945.03	1/1	138.01/8945.03	101.21/32.52	<0.0001*/0.0002*
Residual	13.64/2751.00	10/10	1.36/275.10		
Lack of fit	13.64/2751.00	5/5	2.73/550.20		
Pure error	0.00/0.00	5/5	0.00/0.00		
Cor total	4363.69/140500.00	19/19			

*Significant

the interaction of X_1, X_2 and X_3 on each response, the adequacy of linear, two factor interaction (2FI), quadratic and cubic models were analyzed by sequential model sum of squares (type I) and model summary statistics. From the results of the sequential test, the linear and quadratic models explained the results of TF and SF better than others. Since, the total number of runs in CCD was insufficient to support a full cubic model, it was declared aliased for both the responses [54]. Due to higher adj. R^2 values (0.9628/0.9941 and 0.6672/0.8989 for quadratic and linear models, respectively, of TF/SF) along with better correlation of adj. R^2 and pred. R^2 values, quadratic model was found to be more applicable than linear model (according to the model summary statistics test). Therefore, results of PV experiments were statistically analyzed by quadratic model which evolved the following empirical expressions for TF (Eq. (31)) and SF (Eq. (32)).

$$R_{TF}=-90.408+2.799X_1-11.957X_2+1.477X_3+0.324X_1X_2 -0.356X_1X_3-0.297X_2X_3+0.066X_1^2+0.878X_2^2+0.396X_3^2 \quad (31)$$

$$R_{SF}=75.076-0.298X_1-13.692X_2+3.746X_3+0.087X_1X_2 -0.013X_1X_3-0.135X_2X_3-0.008X_1^2+0.755X_2^2-0.049X_3^2 \quad (32)$$

Applicability of the selected quadratic model was justified from the plot of experimental vs. model generated data, in which very high adj. R^2 values (0.9628/0.9941 for TF/SF) were observed indicating normal distribution of error around the mean (Fig. 6(a), (b)). However, validation of this model in the entire range of variables was verified by fitting some other experimental data to Eqs. (31) and (32) (Fig. 6(c), (d)). Results showed close resemblance of experimental and model generated data, describing better acceptability of the model in the entire range of experiment. Analysis of *F* values indicated that the significant variables for TF as X_1 (*F* value=133.41), X_2 (*F* value=12.80), X_3 (*F* value=221.42), X_1X_3 (*F* value=53.15) and X_3^2 (*F* value=32.52). On the other hand, for SF, the significant variables became X_1 (*F* value=397.03), X_2 (*F* value=710.10), X_3 (*F* value=1818.52), X_1X_2 (*F* value=26.46), X_1X_3 (*F* value=14.69), X_2X_3 (*F* value=92.22), X_2^2 (*F* value=41.46) and X_3^2 (*F* value=101.21) with positive or negative coefficients (Table 3). The response surface effects of X_1, X_2; X_1, X_3 and X_2, X_3 on TF and SF, respectively, are represented in Fig. 6(e)-(j).

From Fig. 6(e) and Fig. 6(h), TF was found to increase from 92.606 to 128.076 g m^{-2} h^{-1} for NRSEV0 with increase in wt% of THF at 35 °C, whereas SF decreased from 32.249 to 18.084 under similar set of experimental conditions. Similarly, TF increased from 39.368 to 96.92 g m^{-2} h^{-1} for NRSEV24 by the increase in temperature from 35 to 55 °C, whereas, SF dropped from 44.348 to 31.812 under identical set of conditions. At higher wt% of THF in feed, plasticization of organophilic membrane resulted in swelling and loosening of the organophilic rubber chains due to the closeness of solubility parameters of rubber membrane and THF. Because of this, permeates were allowed to pass not through a tortuous path. Due to lower molecular diameter, water could pass through this plasticized membrane more rapidly than THF, causing comparatively higher flux of water than THF. Thus, SF was found to decrease with increasing wt% of THF in feed. It was also observed that the rate of increase in TF was more rapid with increasing wt% of THF in the higher temperature region. Conversely, SF decreased more rapidly under an identical set of conditions, possibly due to significant increase of segmental motion by the plasticization of organoselective membranes and subsequently allowing both components to pass through it. Similarly, the rate of increase in TF with temperature was found to be more rapid in the range of higher wt% of THF.

The increase in temperature raised TF from 39.368 to 96.92 g m^{-2} h^{-1}, whereas SF showed an opposite trend to decrease from 44.348 to 31.812, under identical experimental conditions (Fig. 6(f) and Fig. 6(i)). Again, with the increase in temperature, apparent activation energy for THF permeation increased, whereas it remained almost constant for water permeation [31]. Thus, at higher temperature, the mobility of rubber chains allowed more water molecules to diffuse owing to smaller molecular diameter of water (0.265

nm) than THF (0.585 nm) [27]. This resulted an increase in TF at high temperature. In contrast, the increase in filler within the membrane reduced TF accompanied by high SF. In fact, increasing amount of filler loading enhanced physical crosslinking of rubber membranes that reduced free space in the rubber matrix and restricted permeation of both components. This caused a decrease in TF and an increase in SF with increasing filler loading, instead of similar kind of sulfur crosslinking (SEV). As change in TF and SF became almost constant beyond 24 wt% filler loading, no study was performed beyond this limit. However, the combined effect of the filler loading and temperature showed that temperature effect for both TF and SF was more prominent in NRSEV0 than NRSEV24. Again, TF decreased more rapidly from NRSEV0 to NRSEV24 at the higher temperature, whereas the opposite effect was also observed for SF under equivalent set of conditions.

From the combined effect of THF wt% and filler loading on TF and SF (Fig. 6(g) and Fig. 6(j)), TF was found to decrease from 128.076 to 39.368 g m^{-2} h^{-1} with increasing filler loading from NRSEV0 to NRSEV24, whereas SF showed an opposite trend to that of TF. In contrary, TF was enhanced from 92.606 to 128.076 g m^{-2} h^{-1} with the increase in wt% of THF for NRSEV0 at 35 °C, whereas the reverse trend of TF was observed for SF. Also, TF decreased rapidly with increasing filler loading from NRSEV0 to NRSEV12 and beyond this limit, the filler effect became negligible. With the increase in filler loading from NRSEV0 to NRSEV24, TF decreased more rapidly at higher wt% of THF. Conversely, SF was also found to increase more rapidly at much lower wt% of THF in water.

10-1. Validation Test

To justify the applicability of the regressed equations (Eqs. (31) and (32)), a validation test was performed by taking some other values of the input variables which were not included into the data range used in RSM. The predicted responses (TF and SF) were plotted with the experimental data (Fig. 6(c), (d)). The adj. R^2 values for TF/SF were found to be as high as 0.9918/0.9996, which indicated close resemblance of experimental and model generated data. This validation test also indicated the rational applicability of RSM generated quadratic model to explain the PV experiment.

10-2. Optimization

The objective of the present study was to find the optimum conditions of the independent variables to obtain maximum SF, ensuring maximum THF removal from water. The most appropriate condition satisfying the above criteria was found as X_1=35 °C, X_2=2.44% and X_3=24% having maximum SF (76.16) and maximum desirability (0.997) (Fig. 6(k)-(m)).

11. Discussion of Mechanism

Mechanical properties/CDs of vulcanized rubber membranes depend on the sulfidic bridge lengths (mono-/bi-/poly-sulfidic) which are controlled by the introduction of various A/S ratios. EV (A/S=2.50-12.00), SEV (A/S=0.70-2.50) and CV (A/S=0.10-0.60) predominantly produce mono-, bi- and poly-sulfidic linkages, respectively. RSM optimization has established that SEV of NR resulted in the best balance of TS and EAB, which is an essential property of any membrane working under the presence of driving force differential of PV. Thus, a rational mechanism of vulcanization was introduced to remove all ambiguities of it, and all the possible crosslinked products along with the precursors that appeared during the process of crosslinking (Schemes 1 and 2).

Accelerated sulfur crosslinking of NR can be done by using accelerators, like zinc dimethyldithiocarbamate (ZDMC), 2-mercaptobenzothiazole (MBT), dibenzothiazyldisulfide (MBTS), N-cyclohexyl-2-benzothiazolesulfenamide (CBS), zinc dibenzyldithiocarbamate (ZBEC) and zinc(N-methyl-piperazine)dithiocarbamate (ZPDC) of different kinds and varying the A/S ratios [31]. To obtain better properties of NR, it is subjected to vulcanization with different type and amount of accelerators [55,56]. At higher temperature (~110 °C), sulfur vulcanization is extensively carried out in presence of ZDC [27,31]. Rational mechanistic schemes for ZDC accelerated sulfur vulcanization of NR and different crosslinking products via ionic/radical paths are given in Scheme 1/Scheme 2.

11-1. Accelerated Sulfur Vulcanization through Ionic Path

Accelerated vulcanization is initiated by interaction of ZDC and sulfur (S_8) to produce poly-sulfidic homologous of ZDC, which is subsequently fragmented at higher temperature (~110 °C) by heterolytic cleavage of Zn-S bond to form diethylthiocarbamoyl polysulfenium ions (**1**), diethylthiocarbamoyl polysulfide ions (**2**) and zinc sulfide. Diethylthiocarbamoyl polysulfenium ion (**1**) reacts with the π-electrons of NR (**3**) to produce cyclic polysulfonium ions (**4**). The C=S bond of **4** may involve in β-hydrogen abstraction from three nonequivalent allylic positions of the NR moiety followed by internal rearrangement and fragmentation resulting polysulfenium ions (**5**, **6** and **7**). Same rubber moiety, **4** may also undergo base (**2**) assisted β-hydrogen abstraction to produce **8**, **9** and **10**. In another path**,** the formation of **11** is associated through β-hydrogen abstraction by the base (**2**) from the ring of cyclic polysulfonium ions (**4**) of the rubber moiety. Following the same mechanistic pathway crosslinking products (**12a**, **12b**, **12c** to **15a**, **15b**, **15c**) are formed when polysulfenium ions (**5**, **6** and **7**) react with double bond of NR (**3**). These vulcanizing products contain S_x as a crosslink unit forming mono- (n=1), di- (n=2) and poly-sulfidic (n>2) crosslinking in different extent between the two NR chains. The variation of such crosslinking resulted in the change in membrane physicochemical properties as well as performance, which was optimized by RSM.

11-2. Accelerated Sulfur Vulcanization through Radical Path

In a radical path of ZDC accelerated sulfur vulcanization, the poly-sulfidic homologue of ZDC undergoes homolytic cleavage to produce polysulfanyl radical (**16**), which can abstract allylic protons to produce three different types of allylic radicals (**17**, **18** and **19**). The polysulfanyl radical (**16**) can also undergo radical addition to the double bond of unreacted NR (**3**) followed by rearrangement to produce five different polysulfanyl radicals (**20**, **21**, **22**, **23** and **24**). The allylic radicals (**17**, **18** and **19**) undergo radical combination to the NR-polysulfanyl radicals (**20**, **21**, **22**, **23** and **24**), producing crosslinked NR polymeric chains (**25a**, **25b**, **25c** to **29a**, **29b**, **29c**).

12. Comparison of the Results Obtained with those Reported in Literature

Different membranes, including filled and crosslinked natural or synthetic rubbers, blends of rubbers, crosslinked copolymers, graft copolymers, synthetic homopolymers, crosslinked natural polymers etc., have been reported till date for pervaporative removal of THF

Table 4. Comparison of THF removal performance of various pervaporation membranes from THF/water mixtures

Membranes used	Membrane thickness (mm)	Normalized flux (kg mm m^{-2} h^{-1})/ Temperature (°C)/THF in feed (wt%)	Separation factor (-)	Ref.
PP0[a]	50	0.56/30/0.9	125	17
F1[b]	50	0.95/30/0.9	84	17
UPVC[c]	30	0.21/30/0.9	125.00	2
Blend-5[d]	30	0.41/30/0.9	93.94	2
PPVC-5[e]	30	0.63/30/0.9	62.88	2
PSTY[f]	30	0.49/30/0.9	71.97	2
PTMSP–CL[g]	100	9.66/50/5	26.88	19
PAI-g-PDMS1[h]	100-200	39.3/50/6.99	75.4	18
PAI-g-PDMS3[h]	100-200	96.2/50/6.99	120	18
NRSEV0[i]	50±0.55	4.20±0.13/35/0.97	58.51±2.05	TS[#]
NRSEV8	50±0.55	1.96±0.07/35/0.97	97.19±3.40	TS[#]
NRSEV12	50±0.55	1.20±0.03/35/0.97	118.8±4.16	TS[#]
NRSEV24	50±0.55	1.04±0.03/35/0.97	133.96±4.69	TS[#]

[a]Unplasticized polyvinyl chloride membrane
[b]Polyvinyl chloride membrane containing 25 wt% of dioctyl phthalate/1 wt% bentonite clay
[c]Unplasticized polyvinyl chloride
[d]Plasticized polyvinyl chloride
[e]Polystyrene
[f]Blends of UPVC and PSTY
[g]Crosslinked poly[1-(trimethylsilyl)-1-propyne]
[h]Siloxane-grafted poly(amide-imide)
[i]Semi-efficiently vulcanized natural rubber membranes
[#]This study

from THF-water mixtures. A comparative study of membrane performance differing in origin/chemical nature, thickness (30-200 μm), feed concentration of THF (0.9-6.99 wt% of THF) and temperature (35-50 °C) in terms of normalized flux (NF) and SF for rubber membranes has been included in Table 4. SF of this study was the maximum according to the literature. Again, NF depends on temperature, feed concentration of THF, amount of filler loading and membrane thickness. With the increase in feed concentration of THF and/or temperature, enhanced segmental motion of rubber chains allows smoother passing of both components to result higher TF but lower SF. Although the increasing amount of filler restricts permeation, it helps increase in total sorption of the used membranes due to their added organoselective nature in presence of CBF fillers. Despite low temperature, low THF concentration in feed, presence of organophilic fillers and comparable thickness, the used membranes show excellent SF and reasonable normalized flux (NF) using low cost modified natural polymers in low energy pervaporation process.

CONCLUSION

Chemically modified unfilled and composite NR membranes can be used effectively for PV separation of THF from water at different feed compositions and temperature. Mechanical, thermal, spectroscopic, microscopic and diffractometric methods have been used to characterize these mixed-matrix membranes. These mechanically strong and dimensionally stable rubber membranes can extensively be used for the separation of any organic-water mixtures, where the solubility parameter of component to be permeated is close to the elastomeric membranes. Membrane having A/S=0.9898 shows the best balance of TS and EAB. However, the ultimate optimum membrane performance was obtained by two stages RSM based statistical optimization (property and performance) at A/S=0.989 and 24 wt% of fillers. We also measured the mere and interactive effects of filler, temperature and concentration on TF and SF. NRSEV24 shows the highest SF (133.96±4.69), while in terms of both TF and SF, NRSEV12 (31.68±0.92 g m^{-2} h^{-1} and 67.34±2.36, respectively) shows optimum performance. Membrane intrinsic properties, like PPs, MSs and DCs, were studied to avoid the membrane property variation with such variables. Coupling effects of sorption, in terms of state-I, state-II and state-III activity coefficients, were also studied by Flory-Huggins thermodynamics. Physical and chemical crosslink densities, solubility parameters, TS, EAB, modulus and interaction parameters were found to vary with chemical crosslinking and filler loading. The present work describes rationally all possible NR-based crosslinked membranes, formed from crosslinking precursors in accelerated sulfur vulcanization mechanism through radical and/or ionic paths and formation of crosslinks by reactions involving H-abstraction, radical addition, radical-radical coupling and sulfur-transfer, to remove ambiguities of the reaction mechanism. The newly developed method of property/performance optimization can also be implemented for pervapora-

tive separation of organics and dehydration by using peroxide/resol cured saturated/unsaturated synthetic rubber (e.g. SBR, EPDM and PDMS) membranes. Finally, in the field of computational quantum mechanical modelling method, used in chemistry, chemical technology, physics and material science, the comprehensive mechanistic studies of rubber vulcanization, comprising several intermediates and pathways to establish the reaction mechanism, can also provide an innovative idea and impetus to find the transition state(s), optimized structure(s) and activation energies through *ab initio* parametrization of density functional theory (DFT). In terms of its simple modification, performance characteristics, application prospects and diversities, these natural, polymer based CBF filled and vulcanized membranes show the novelty and versatility to be used in the separation of traces of organics, like THF, pyridine, toluene, dioxane, MTBE etc. from water. These low cost unfilled (NRSEV0) as well as composite membranes (NRSEV8, NRSEV12 and NRSEV24) can be an attractive replacement of conventionally used polymeric membranes in energy saving and environment friendly green separation process with no emission of chemicals.

ACKNOWLEDGEMENTS

The corresponding author gratefully acknowledges the DST, Government of India (YSS/2015/000886) and DST, Government of West Bengal (773(Sanc.)/ST/P/S&T/15G-2/2015) for their financial assistance and the Department of Higher Education, Government of West Bengal for providing the opportunity to participate in inter-institutional collaboration with University of Calcutta. Second author is grateful to UGC, Government of India for providing fellowship.

SUPPORTING INFORMATION

Additional information as noted in the text. This information is available via the Internet at http://www.springer.com/chemistry/journal/11814.

REFERENCES

1. J. Wang, W. Zhang, W. Li and W. Xing, *Korean J. Chem. Eng.*, **32**, 1369 (2015).
2. S. Ray, N. R. Singha and S. K. Ray, *Chem. Eng. J.*, **149**, 153 (2009).
3. N. R. Singha, S. Ray, S. K. Ray and B. B. Konar, *J. Appl. Polym. Sci.*, **121**, 1330 (2011).
4. C. Yeom, J. M. Dickson and M. A. Brook, *Korean J. Chem. Eng.*, **13**, 482 (1996).
5. K. Koczka, J. Manczinger, P. Mizsey and Z. Fonyo, *Chem. Eng. Process.*, **46**, 239 (2007).
6. B. L. Lucht and D. B. Collum, *Acc. Chem. Res.*, **32**, 1035 (1999).
7. C. Elschenbroich and A. Salzer, in *Oganometallics - A Concise Introduction*, A. Fürstner Eds., *Verlagsgesellschaft* mbH, *Weinheim* (1996).
8. P. Chapman, X. X. Loha, A. G. Livingston, K. Lia and T. A. C. Oliveira, *J. Membr. Sci.*, **309**, 102 (2008).
9. S. Ray and S. K. Ray, *Chem. Eng. Process.*, **47**, 1620 (2008).
10. M. D. Kurkuri, J. N. Nayak, M. I. Aralaguppi, B. V. K. Naidu and T. M. Aminabhavi, *J. Appl. Polym. Sci.*, **98**, 178 (2005).
11. B. V. K. Naidu, K. S. V. K. Rao and T. M. Aminabhavi, *J. Membr. Sci.*, **260**, 131 (2005).
12. P. S. Rao, S. Sridhar and A. Krishnaiah, *J. Appl. Polym. Sci.*, **102**, 1152 (2006).
13. M. Sairam, B. V. K. Naidu, S. K. Nataraj, B. Sreedhar and T. M. Aminabhavi, *J. Membr. Sci.*, **283**, 65 (2006).
14. S. D. Bhat and T. M. Aminabhavi, *Sep. Purif. Technol.*, **51**, 85 (2006).
15. P. D. Chapman, X. Tan, A. G. Livingston, K. Lia and T. Oliveira, *J. Membr. Sci.*, **268**, 13 (2006).
16. J. G. Varghese, A. A. Kittur and M. Y. Kariduraganavar, *J. Appl. Polym. Sci.*, **111**, 2408 (2009).
17. P. Das and S. K. Ray, *J. Ind. Eng. Chem.*, **34**, 321 (2016).
18. Y. Nagase, T. Ando and C. M. Yun, *React. Funct. Polym.*, **67**, 1252 (2007).
19. S. Claes, P. Vandezande, S. Mullens, P. Adriaensens, R. Peeters, F. H. J. Maurer and M. K. V. Bael, *J. Membr. Sci.*, **389**, 459 (2012).
20. A. F. Ismail and P. Y. Lai, *Sep. Purif. Technol.*, **40**, 191 (2004).
21. A. Idris, F. Kormin and M. Y. Noordin, *Sep. Purif. Technol.*, **49**, 271 (2006).
22. F. Xiangli, W. Wei, Y. Chen, W. Jin and N. Xu, *J. Membr. Sci.*, **311**, 23 (2008).
23. V. García, J. L. Aguirre, E. Pongrácz, P. Perämäki and R. L. Keiski, *J. Membr. Sci.*, **338**, 111 (2009).
24. M. Mahapatra, M. Karmakar, B. Mondal and N. R. Singha, *RSC Adv.*, **6**, 69387 (2016).
25. D. Dondi, A. Buttafava, A. Zeffiro, C. Palamini, A. Lostritto, L. Giannini and A. Faucitano, *Eur. Polym. J.*, **62**, 222 (2015).
26. J. R. Wolfe Jr., *Rubber Chem. Technol.*, **41**, 1339 (1968).
27. N. R. Singha and S. K. Ray, *J. Appl. Polym. Sci.*, **124**, E99 (2012).
28. S. D. Bhat and T. M. Aminabhavi, *J. Membr. Sci.*, **306**, 173 (2007).
29. H. S. Samanta, S. K. Ray, P. Das and N. R. Singha, *J. Chem. Technol. Biot.*, **87**, 608 (2012).
30. R. W. Baker, J. G. Wijmans and Y. J. Huang, *J. Membr. Sci.*, **348**, 346 (2010).
31. N. R. Singha, P. Das and S. K. Ray, *J. Ind. Eng. Chem.*, **19**, 2034 (2013).
32. E. W. Greenlaw, W. D. Prince, R. A. Shelden and E. V. Thompson, *J. Membr. Sci.*, **2**, 141 (1977).
33. J. Hao, K. Tanaka and H. Kita, *J. Membr. Sci.*, **132**, 97 (1997).
34. Y. Fukahori, *Rubber Chem. Technol.*, **80**, 701 (2007).
35. A. Schröder, M. Klüppel and R. H. Schuster, *Macromol. Mater. Eng.*, **292**, 885 (2007).
36. M. A. Montes-Morán, D. Suárez, J. A. Menéndez and E. Fuente, *Carbon*, **42**, 1219 (2004).
37. A. Barroso-Bogeat, M. Alexandre-Franco, C. Fernández-González and V. Gómez-Serrano, *Energy Fuel*, **28**, 4096 (2014).
38. J. B. Donnet and A. Voet, *Carbon Black: Physics, Chemistry, and Elastomer Reinforcement*, Marcel Dekker, New York (1976).
39. N. R. Singha, T. K. Parya and S. K. Ray, *J. Membr. Sci.*, **340**, 35 (2009).
40. A. Asfaram, M. Ghaedi, S. Hajati, A. Goudarzi and A. A. Bazrafshan, *Spectrochim. Acta. A.*, **145**, 203 (2015).
41. S. Chatterjee, A. Kumar, S. Basu and S. Dutta, *Chem. Eng. J.*, **181-182**, 289 (2012).
42. B. H. Hameed, I. A. W. Tan and A. L. Ahmed, *J. Hazard. Mater.*, **158**, 324 (2008).
43. J. N. Sahu, J. Acharya and B. C. Meikap, *J. Hazard. Mater.*, **172**, 818

(2009).
44. S. J. Lue, W. W. Chen, and S. F. Wang, *Separ. Sci. Technol.*, **44**, 3412 (2009).
45. P. Li, L. Yin, G. Song, J. Sun, L. Wang and H. Wang, *Appl. Clay Sci.*, **40**, 38 (2008).
46. N. Tomer, F. D. Jestin, R. Singh and J. Lacoste, *Polym. Degrad. Stab.*, **92**, 457 (2007).
47. R. Stephen, S. Jose, K. Joseph, S. Thomas and Z. Oommen, *Polym. Degrad. Stab.*, **91**, 1717 (2006).
48. H.Nabil, H. Ismail and A. R. Azura, *Mater. Design.*, **53**, 651 (2014).
49. H. Darmstadt, C. Roy, S. Kaliaguine, G. Xu, M. Auger, A. Tuel and V. Ramaswamy, *Carbon*, **38**, 1279 (2000).
50. C. C. Wang, J. B. Donnet, T. K. Wang, M. P. Johnson and F. Welsh, *Rubber Chem. Technol.*, **78**, 17 (2005).
51. W. Kemp, *Organic Spectroscopy*, Macmillan Education Ltd., Hampshire (1991).
52. N. R. Singha, S. Kar, S. Ray and S. K. Ray, *Chem. Eng. Process.*, **48**, 1020 (2009).
53. M. Iqbal, N. Iqbal, I. A. Bhatti, N. Ahmed and M. Zahid, *Ecol. Eng.*, **88**, 265 (2016).
54. D. C. Montgomery, *Design and Analysis of Experiments*, Wiley, New York (2013).
55. A. S. Aprem, K. Joseph, T. Mathew, V. Altstaedt and S. Thomas, *Eur. Polym. J.*, **39**, 1451 (2003).
56. P. Ghosh, S. Katare, P. Patkar, J. M. Caruthers and V. Venkatasubramanian, *Rubber Chem. Technol.*, **76**, 592 (2003).

Supporting Information

Separation of tetrahydrofuran using RSM optimized accelerator-sulfur-filler of rubber membranes: Systematic optimization and comprehensive mechanistic study

Mrinmoy Karmakar, Manas Mahapatra, and Nayan Ranjan Singha†

Department of Polymer Science and Technology, Advanced Polymer Laboratory,
Government College of Engineering and Leather Technology (Post-Graduate),
Maulana Abul Kalam Azad University of Technology, Salt Lake, Kolkata - 700106, West Bengal, India
(*Received 1 October 2016 • accepted 6 February 2017*)

1. Effect of Feed Temperature on Fugacity, Membrane Selectivity (MS) and Partial Permeability (PP) of THF and Water

As observed in Fig. S1(c), PPs of THF were found to decrease with the rise in temperature, whereas PPs of water followed an opposite trend. In fact, segmental motion of the rubber chains as well as mobility of the permeants increased the free volume of membrane, resulting an increase in partial fluxes. However, the rate of increase in fugacity (Fig. 5(b)) was found to be more than that of THF, causing a decrease in THF PP. Since PPs of THF fall rapidly than water, MSs were found to decrease (Fig. S1(b)) from 5.26±0.17 to 1.06±0.04 with the rise in temperature at 0.97 wt% of THF in feed. Altogether, PPs of THF/water was observed to vary from $(31.06\pm0.99)\times10^{-8}/(9.67\pm0.31)\times10^{-8}$ to $(7.54\pm0.26)\times10^{-8}/(19.57\pm0.63)\times10^{-8}$ Barrer with the rise in temperature from 35 to 55 °C at 0.97 wt% of THF in feed.

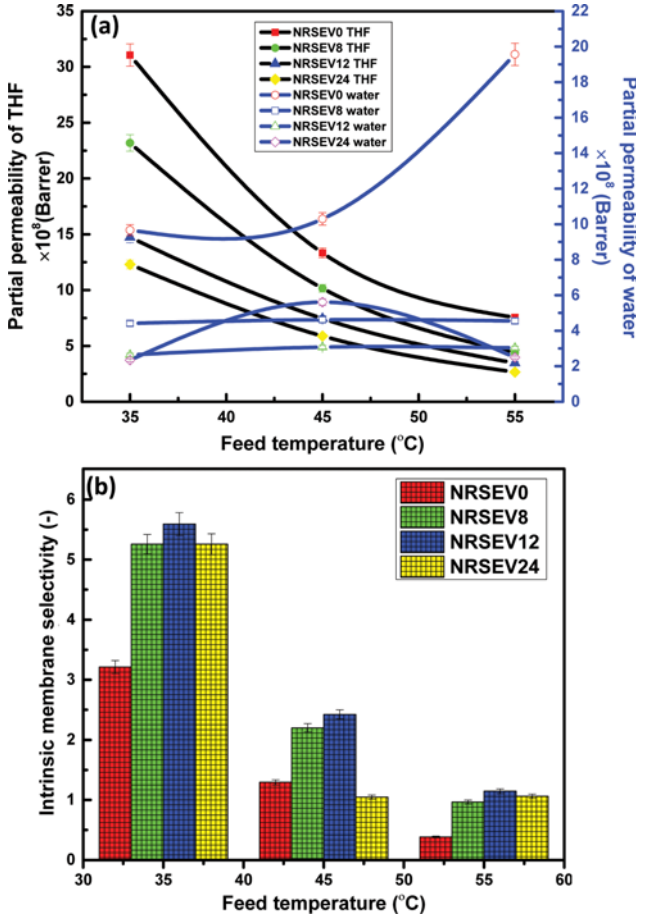

Fig. S1. Effect of feed temperature on partial permeability (a) and membrane selectivity (b) of THF and water.

Table S1. Design matrix and response data for TS and EAB

Runs	Uncoded values		TS (MPa)		EAB (%)	
	P (wt%)	Q (wt%)	Actual	Predicted	Actual	Predicted
1	2.00	3.00	5.20	5.17	460.00	461.74
2	8.00	3.00	8.54	8.54	324.00	325.91
3	2.00	6.00	4.44	4.40	540.00	539.91
4	8.00	6.00	8.44	8.43	355.00	355.07
5	2.00	4.50	4.73	4.80	510.00	508.36
6	8.00	4.50	8.50	8.50	350.00	348.02
7	5.00	3.00	8.11	8.14	390.00	386.36
8	5.00	6.00	7.65	7.70	440.00	440.02
9	5.00	4.50	7.95	7.93	420.00	420.72
10	5.00	4.50	7.95	7.93	420.00	420.72
11	5.00	4.50	7.95	7.93	420.00	420.72
12	5.00	4.50	7.95	7.93	420.00	420.72
13	5.00	4.50	7.95	7.93	420.00	420.72

Table S2. ANOVA for TS and EAB

Source	Sum of squares	Df^	Mean square	*F* value	*P*-value
Model	26.33/ 43705.59	5/5	5.27/8741.12	3077.97/2097.25	<0.0001*/<0.0001*
P	20.57/38560.17	1/1	20.57/38560.17	12022.22/9251.71	<0.0001*/<0.0001*
Q	0.29/4320.17	1/1	0.29/4320.17	169.71/1036.53	<0.0001*/<0.0001*
PQ	0.11/600.25	1/1	0.11/600.25	63.64/144.02	<0.0001*/<0.0001*
P^2	4.54/153.93	1/1	4.54/153.93	2652.30/36.93	<0.0001*/ 0.0005*
Q^2	7.88×10^{-4}/156.79	1/1	7.88×10^{-4}/156.79	0.46/37.62	0.5191/ 0.0005*
Residual	0.012/29.18	7/7	1.711×10^{-3}/4.17		
Lack of fit	0.012/29.18	3/3	3.993×10^{-3}/9.73		
Pure error	0.00/0.00	4/4	0.00/0.00		
Cor total	26.35/43734.77	12/12			

*Significant and ^degrees of freedom

Table S3. Design matrix and response data for SF and TF

	Coded/uncoded values			Experimental/ Predicted responses (SF)	Experimental/ Predicted responses (TF)
	Temperature (°C)	Wt% of THF	Wt% of filler		
1	0/45	0/4.89	0/12	38.86/38.66	68.22/71.36
2	0/45	0/4.89	0/12	38.86/38.66	68.22/71.36
3	0/45	0/4.89	0/12	38.86/38.66	68.22/71.36
4	0/45	−1/2.44	0/12	53.25/55.32	54.73/57.02
5	−1/35	−1/2.44	+1/24	76.16/76.36	39.19/24.61
6	+1/55	+1/734	+1/24	30.64/31.81	94.88/96.92
7	0/45	+1/7.34	−1/0	16.03/17.41	203.30/183.09
8	−1/35	0/4.89	0/12	45.44/45.90	14.25/35.82
9	−1/35	0/4.89	−1/0	17.54/18.08	131.40/128.08
10	+1/55	+1/7.34	+1/24	54.03/53.34	58.95/64.62
11	−1/45	−1/2.44	+1/24	47.52/46.72	47.21/58.06
12	+1/55	0/4.89	−1/0	10.24/9.89	353.96/370.90
13	0/45	+1/7.34	0/12	38.86/38.66	68.22/71.36
14	−1/35	0/4.89	+1/24	44.27/44.39	43.33/39.37
15	0/45	+1/7.34	0/12	33.54/32.05	92.25/80.6
16	−1/35	+1/7.34	−1/0	33.57/32.25	92.29/92.61
17	0/45	−1/2.44	0/12	38.86/38.66	68.22/71.36
18	0/45	0/4.89	0/12	38.86/38.66	68.22/71.36
19	+1/55	−1/2.44	−1/0	17.51/17.51	283.05/289.37
20	+1/55	0/4.89	0/12	30.72/30.84	135.41/104.48

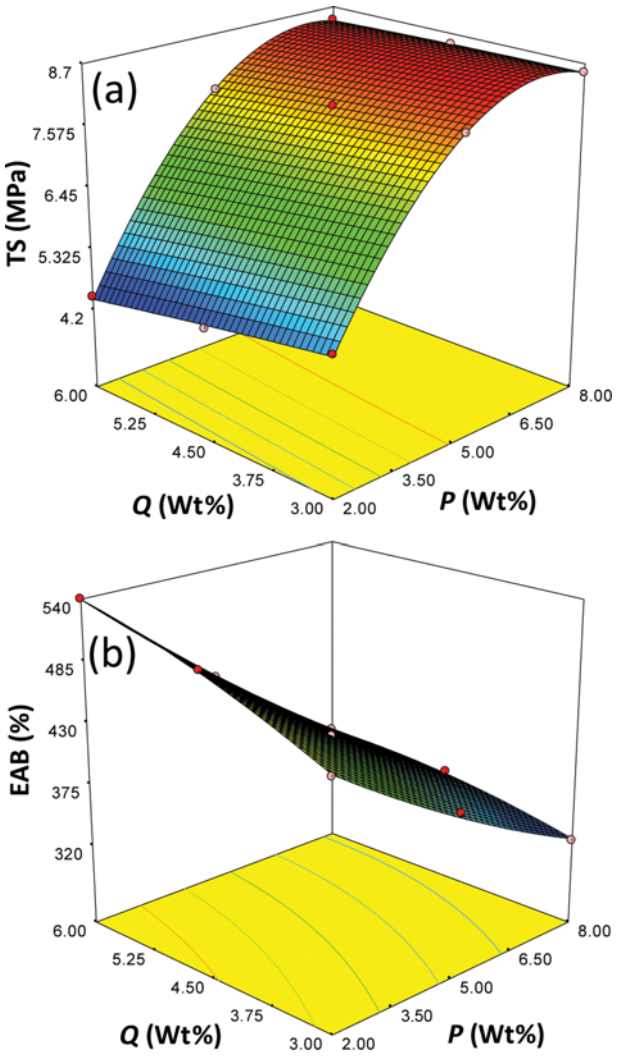

Fig. S2. 3D response surface plots of TS (a) and EAB (b).

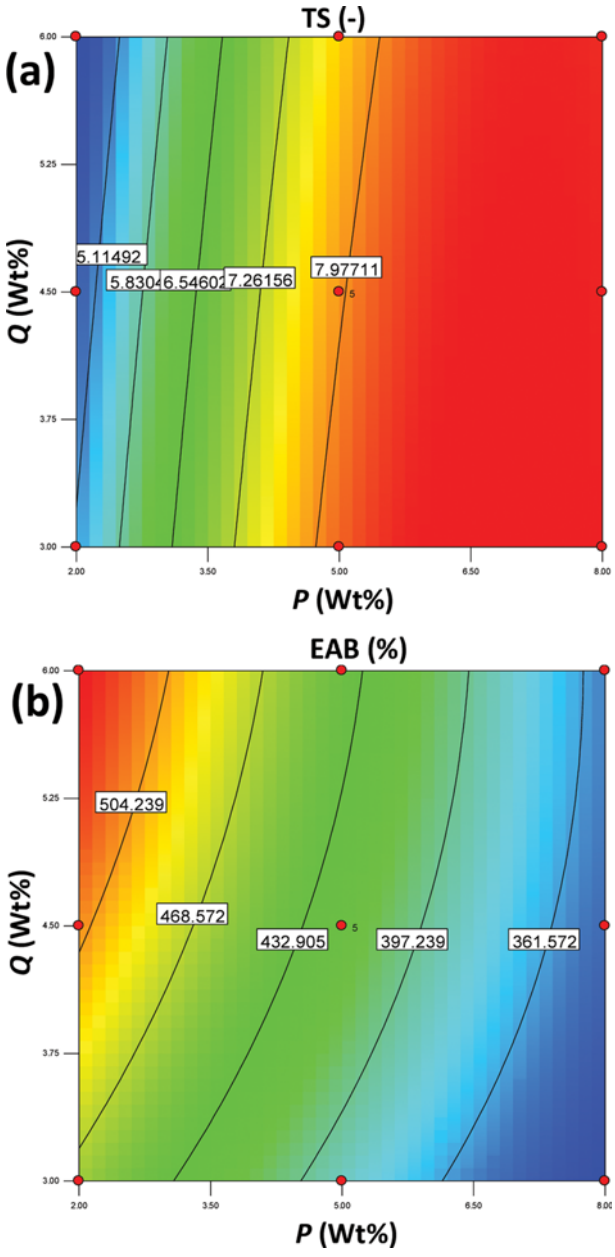

Fig. S3. 2D contour plots of TS/EAB vs. wt% of S/wt% of accelerator (a/b).